

The triple oxygen isotope composition of Precambrian chert

Frasier L. Liljestrand^{a,1}, Andrew H. Knoll^a, Nicholas J. Tosca^b, Phoebe A. Cohen^c, Francis A. Macdonald^d, Yongbo Peng^e, David T. Johnston^{a,1}

^a*Department of Earth and Planetary Sciences, Harvard University, Cambridge, MA, 02138, USA*

^b*Department of Earth Sciences, University of Oxford, Oxford, OX13AN, UK*

^c*Department of Geosciences, Williams College, Williamstown, MA, 01267, USA*

^d*Department of Earth Science, UC Santa Barbara, Santa Barbara, CA, 93106, USA*

^e*Department of Geology Geophysics, Louisiana State University, Baton Rouge, LA, 70803, USA*

Abstract

The temperature and chemistry of early seawater have both been inferred from the isotopic composition of Precambrian chert (SiO_2), a precipitated mineral formed on or within marine sediments. The $\delta^{18}\text{O}$ of chert shows a robust quasi-linear increase through time - a signal that has been interpreted in a number of conflicting ways. For example, changing $\delta^{18}\text{O}$ has been hypothesized to reflect the product of cooling surface ocean temperatures, a signature of evolving seawater $\delta^{18}\text{O}$ composition, or the product of later stage diagenesis (where measured $\delta^{18}\text{O}$ reflects the composition of diagenetic fluids). We suggest this uncertainty can be resolved through the additional measurement and interpretation of the minor oxygen isotope ^{17}O (noted as $\Delta^{17}\text{O}$) in conjunction with $\delta^{18}\text{O}$. In this study, we present a suite of triple oxygen isotope data on stratigraphically constrained Precambrian chert (both peritidal chert nodules in carbonates and iron formation silica). These mineralogically well-defined data allow for the first stratigraphic tests of the fidelity of ^{17}O in SiO_2 . We then apply a Monte Carlo resampling technique to test the features of the competing hypotheses noted above, here now including critical constraints from ^{17}O . The most parsimonious interpretation of these data suggests that secondary alteration with higher-temperature,

Email addresses: liljestrand@fas.harvard.edu (Frasier L. Liljestrand), johnston@eps.harvard.edu (David T. Johnston)

meteoric-derived groundwater has skewed an original geochemical signature. This treatment can allow for some change in the oxygen isotope composition of seawater itself, however this does not appear to be the most statistically defensible single solution - clearly, some combination of multiple mechanisms is always possible and even likely. What is definitively the case is an equitable, modern-like Archean surface ocean temperature.

Keywords: Oxygen isotope, Chert

1. Introduction

The temperature-dependence of the oxygen isotope equilibrium between chemical sediments and seawater was one of the first and still most profound ways isotope geochemistry has been applied toward the understanding of past environments [1]. Famously, the $\delta^{18}\text{O}$ record of foraminiferal carbonates was successfully used to determine the temperature and glacial history of the Cenozoic Era [2, 3]. Deeper in Earth's history, however, it becomes harder to uniquely identify a single process or equilibrium capable of explaining observed secular changes in $\delta^{18}\text{O}$ records. For example, it is widely argued (though also debated) that the Precambrian carbonate $\delta^{18}\text{O}$ record is prone to diagenetic alteration [4], which over-writes the primary signal of the depositional environment [5].

Sedimentary chert (SiO_2) precipitates in temperature-dependent isotope equilibrium with the surrounding seawater or pore waters, and the 3500 million year geologic record of chert $\delta^{18}\text{O}$ captures a structured, quasi-linear increase in preserved compositions [6]. Chert is hypothesized to be more resistant to diagenetic alteration than carbonate (or other phases) and so

18 may provide a more reliable record of Proterozoic and Archean environments
19 [7]. This is not to suggest that chert is a perfect recorder, as nodules are
20 commonly polygenic [8], however structured long term variance suggests any
21 $\delta^{18}\text{O}$ alteration is likely second-order to the overall temporal signal. Most
22 directly, the equilibrium temperature-dependence of chert has been used to
23 suggest evolving sea surface temperatures, from a hot Archean world towards
24 our present, equitable climate [7, 9]. Alternatively, however, the same $\delta^{18}\text{O}$
25 record can be explained as a proportional change in the $\delta^{18}\text{O}$ of seawater
26 without invoking any change in surface ocean (i.e. precipitation) temperature
27 [10, 11, 12]. Finally, the chert $\delta^{18}\text{O}$ record could reflect progressive diagenetic
28 alteration, overprinting original depositional signals [13]. Of course, each of
29 the three hypothesis is consistent with the chert record, as they are derived
30 directly from it. Thus, additional $\delta^{18}\text{O}$ observations are unlikely to resolve
31 mechanistic questions about the genesis of this record.

32 Previous research has attempted to address this challenge by coupling the
33 oxygen isotope composition of cherts with other, independent constraints on
34 either temperature or the oxygen isotope composition of seawater. The δD
35 [7, 14] and $\delta^{30}\text{Si}$ records of chert [15], and the $\delta^{18}\text{O}$ record of phosphates
36 [16] have all been invoked as Precambrian temperature proxies, but these
37 techniques, while informative, have not resolved the debate. The clumped
38 isotope record of carbonates has been used to constrain the temperature
39 and $\delta^{18}\text{O}$ of Phanerozoic seawater [17], but has yet to provide as sharp of
40 conclusions in the Precambrian [18, 19, 20, 17]. Most recently, the $\delta^{18}\text{O}$ of

41 sedimentary hematite and goethite [21] suggest changes in the $\delta^{18}\text{O}$ of sea-
 42 water, and related, the triple oxygen isotope composition of bulk shale [22]
 43 point to changes in terrestrial water cycle and associated isotopic composi-
 44 tions. Here, iron minerals carry a lesser temperature dependence on oxygen
 45 isotope fractionation, whereas shale data represent a composite of multiple
 46 oxygen-bearing phases and complexities therein. In parallel, triple oxygen
 47 isotope analysis of altered crustal materials, and ensuing models suggest no
 48 change in seawater composition, but rather offer a revision to oceanic crust
 49 interactions through time [23, 24]. With a suite of opposing interpretations
 50 derived from similar data, the underlying source of the chert $\delta^{18}\text{O}$ signal is
 51 therefore still uncertain.

52 Measuring the $^{16,17,18}\text{O}$ of Precambrian chert may provide important new
 53 insight in this debate. Detailed, high-precision work on geological oxides re-
 54 veals that chemical sediments carry a resolvable mass-dependent signal that
 55 is most sensibly related to the minerals' life histories [25, 22, 23]. The same
 56 temperature-dependent equilibrium isotope effects that have been argued to
 57 explain the $\delta^{18}\text{O}$ of chert have strict, and definitive, predictions for the com-
 58 panion ^{17}O signal. With that in mind, we report the triple oxygen isotope
 59 compositions of a suite of isotopically, mineralogically, and stratigraphically
 60 characterized Precambrian chert. The mass-dependent variations in ^{17}O pro-
 61 vide an additional axis of variation with which to interpret these now classic
 62 $\delta^{18}\text{O}$ records and allow us to distinguish among the three primary hypotheses
 63 advanced to explain $\delta^{18}\text{O}$ records.

64 2. Methods

65 2.1. Isotope notation

66 The ^{17}O of oxygen-bearing minerals is not routinely measured, as it is
67 often assumed that the $\delta^{17}\text{O}$ carries a constant, mass-dependent offset from
68 the $\delta^{18}\text{O}$. As a result, the extra effort required to acquire ^{17}O data was
69 long thought to carry no additional interpretable signal [26]. However, high-
70 precision fluorination methods have changed this mindset, whereby mass laws
71 and additional information can be gleaned from ^{17}O measurements on mass-
72 dependent materials. A suite of simple terms then allows for these small
73 mass-dependent effects be quantified and represented visually. At its most
74 simple, the relationship between ^{17}O and ^{18}O during a fractionating process
75 is described by the equation:

$$^{17}\alpha_{A-B} = (^{18}\alpha_{A-B})^\lambda \quad (1)$$

76 where

$$^x\alpha_{A-B} = \frac{^xR_A}{^xR_B}. \quad (2)$$

77 Here, R is the ratio of the heavy isotope relative to ^{16}O . The λ is the iso-
78 tope effect of ^{18}O compared to ^{17}O for a specific reaction. Values for λ are
79 approximately 0.5, but vary at the percent level as a function of process
80 and temperature [27, 28]. These values range from $\lambda = 0.5305$ for high-
81 temperature equilibrium [28] down to $\lambda \approx 0.5$ for the kinetic fractionation

82 of massive oxygen bearing compounds and forces like gravity [27]. These
 83 different mass laws then manifest as resolvable and measurable anomalies at
 84 the ppm level and presented in standard delta notation:

$$\delta^x O = \left(\frac{\left(\frac{xO}{^{16}O} \right)_{sample}}{\left(\frac{xO}{^{16}O} \right)_{standard}} - 1 \right) * 1000 \quad (3)$$

85 where x is 17 or 18. In order to visualize small variants, $\Delta^{17}O$ is employed.
 86 Here,

$$\Delta^{17}O = 1000 * \left(\ln \left(\frac{\delta^{17}O_{VSMOW}}{1000} + 1 \right) - \lambda_{RL} * \ln \left(\frac{\delta^{18}O_{VSMOW}}{1000} + 1 \right) \right) \quad (4)$$

87 where λ_{RL} is the reference line to which the $\delta^{17}O_{VSMOW}$ values are normal-
 88 ized. We chose to calculate $\Delta^{17}O$ using a λ_{RL} of 0.5305 because it is a
 89 value derived from a thermodynamic prediction, not the average slope of a
 90 set of natural samples, and will therefore not change as a consequence of
 91 increased or improved measurements. All data provided is placed on a VS-
 92 MOW scale by replicate measurement of three common calibrated silicates
 93 (NBS-28, GMG, and San Carlos Olivine) and anchoring on a GMG value of
 94 5.99 and -0.102 $\delta^{18}O$ and $\Delta^{17}O$, respectively [29, 30, 25, 31, 32, 33, 34, 35].

95 2.2. Sample suite

96 The target of this work is to assay the long-term change in the oxygen
 97 isotopic composition of Precambrian chert in order to evaluate its informa-

tion richness. To do so, we collected and analyzed 90 chert-bearing samples that range in age from early Paleoproterozoic to Cambrian, with highest sample density in the Neoproterozoic (see supplemental tables). Within the Neoproterozoic stratigraphy, we also target and perform a stratigraphic test. From these samples, we sub-sampled some rocks with distinct chert phases or nodules, resulting in 105 total sample measurements. Importantly, all these target localities predate the advent of biologically driven opal precipitation, and as such reflect chemical (abiotic) precipitation [36].

A full sample list and locality information is included within the supplement, however two depositional environments dominate the stratigraphy represented. First, most Proterozoic samples reflect peritidal environments, where they precipitated as nodules during early diagenesis [37]. In such environments, supersaturated silica forms an amorphous gel which matures into microcrystalline quartz [38]. Due to the early crystallization, the host fluid in these sediments is often assumed to be comparable in temperature and isotopic composition to the overlying ocean. These are also environments of exceptional microfossil preservation, demonstrating the robust nature of these nodules to post-depositional processes [39]. Juxtaposed to these settings, we also include chert from early Proterozoic and Archean iron formations. Here, the exact depositional environment can vary but is generally basinal, with silica adsorbed onto iron-bearing precipitates from seawater [40, 41, 42, 43]. Other early Archean chert reflect diagenetic alteration of primary sediments, at least in part under the influence of hydrothermal fluids [44].

121 *2.3. chemical methods*

122 The goal in the chemical pre-processing of each sample was to isolate the
123 quartz fraction from any contaminating oxygen bearing phases. For each
124 sample, approximately 1 gram of chert was subsampled and powdered us-
125 ing a tungsten carbide shatterbox. Where texturally appropriate, multiple
126 subsamples were powdered to access separate nodules or visually distinct tex-
127 tures. The powdered samples were acidified in 2 N HCl to remove carbonate
128 phases, then filtered, dried, and baked at 500°C to remove organic matter.
129 This leaves a SiO₂ rich insoluble residue. Detailed mineralogy, on both the
130 pre- and post- acidified samples were conducted at Oxford University (see
131 supplemental tables).

132 The $\delta^{18}\text{O}$ and $\delta^{17}\text{O}$ of the SiO₂ were measured by laser fluorination at
133 Louisiana State University [45] and Harvard University [35]. At LSU, the
134 samples are prefluorinated overnight in a reaction chamber under a BrF₅ at-
135 mosphere, and then heated by a 30 W CO₂-laser to generate O₂. This laser
136 fluorination converts structural oxygen to O₂ gas, which is then separated
137 from excess BrF₅ and other fluorinated byproducts through a series of liquid
138 nitrogen cryo-focusing steps. The O₂ yield, calculated by comparing O₂ pres-
139 sure to the initial mass of chert, is consistently above 90%. The purified O₂ is
140 introduced into a separate Finnigan MAT 253 isotope ratio mass spectrom-
141 eter and analyzed in dual inlet mode. Measurements of silicate standards,
142 NBS-28, UWG-2, and San Carlos Olivine, suggest a reproducibility of 0.3‰
143 and 0.018‰ for $\delta^{18}\text{O}$ and $\Delta^{17}\text{O}$, respectively. At Harvard, the samples are

again prefluorinated overnight, but combusted by a 50 W CO₂-laser under a pure F₂ atmosphere. Sample purification is similar to above, however with the inclusion of an in-line gas chromatograph before being directly introduced to a Thermo Scientific MAT 253 gas source isotope ratio mass spectrometer. Repeated measurements of the same silicate standards generated a reproducibility of 0.4‰ and 0.015‰ for $\delta^{18}\text{O}$ and $\Delta^{17}\text{O}$, respectively. For chert samples analyzed via both methods, the agreement is well under the quoted, conservative, estimates of error from silicate standards (Figure S1, Table S1).

3. Results

In the present study, we add to the existing Precambrian record of $\delta^{18}\text{O}$ in chert and expand by including the minor oxygen isotope, ^{17}O . As seen in Figure 1, the new measurements of $\delta^{18}\text{O}$ align with previous work. Although the exact nature of the change in $\delta^{18}\text{O}$ through time is debated, the progressive increase in $\delta^{18}\text{O}$ is clear. As our new measurements also capture this trend, the accompanying ^{17}O data can confidently be used to assess the source of the full oxygen isotope signal.

It is critical to appreciate that the fluorination methods used here will access all oxygen-bearing phases within a sample, including any contaminants. As such, we begin with an evaluation of the mineralogical content of the targeted material (Figure 2). Here, about 80% of the chemically treated samples consisted of more than 90% quartz. Our chemical preparation method effectively removed carbonate, but the remaining 20% of samples had significant

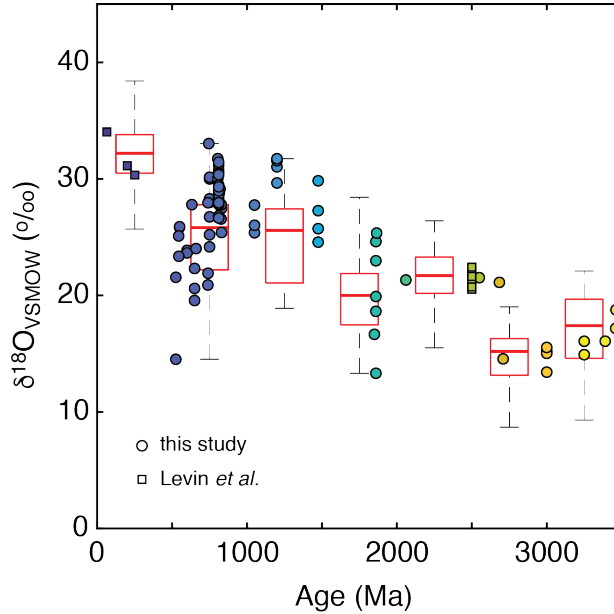


Figure 1: The $\delta^{18}\text{O}$ of chert (‰) relative to Vienna Standard Mean Ocean Water plotted as a function of time. Data points are $\delta^{18}\text{O}$ measurements of chert for which $\Delta^{17}\text{O}$ measurements are available (circles from this study, squares from [25]). Box and whisker plots are additional $\delta^{18}\text{O}$ measurements from previous studies grouped in 500 Ma bins [6]. The central red line shows median value, the box represents the 25th and 75th percentile, the whiskers are 1.5 times the scale of the box. The color coding of the data corresponds to the age of the sample (x axis) and is consistent in subsequent figures. A similar plot highlighting the ^{17}O data is presented in Figure S2.

166 fractions of primarily clay and iron oxide. These other oxygen bearing phases
 167 risk contaminating the primary SiO_2 signal. In fact, samples with significant
 168 non-silica phases are on average 7.2‰ lighter in $\delta^{18}\text{O}$ (and only 0.02‰ heav-
 169 ier in $\Delta^{17}\text{O}$). We thus focus only on the samples with greater than 90%
 170 quartz fraction. It is noteworthy that other environmentally relevant infor-
 171 mation could be locked within these coexisting mineral phases. The complete
 172 mineralogy data is presented in Supplemental materials.

173 From the now curated dataset, a clear secular increase in the $\delta^{18}\text{O}$ of

174 chert is apparent, from Archean compositions averaging below 20‰ toward
 175 late Precambrian values above 30‰ (Figure 1). The corresponding $\Delta^{17}\text{O}$
 176 composition is consistently negative, ranging from -0.04 to -0.26 ‰. The
 177 negative values are a product of our using $\lambda = 0.5305$, the maximum possible
 178 slope, as our reference when calculating $\Delta^{17}\text{O}$ and are consistent with the
 179 existing literature data [25]. The isotope measurements are presented in
 180 supplemental files and Figure 2.

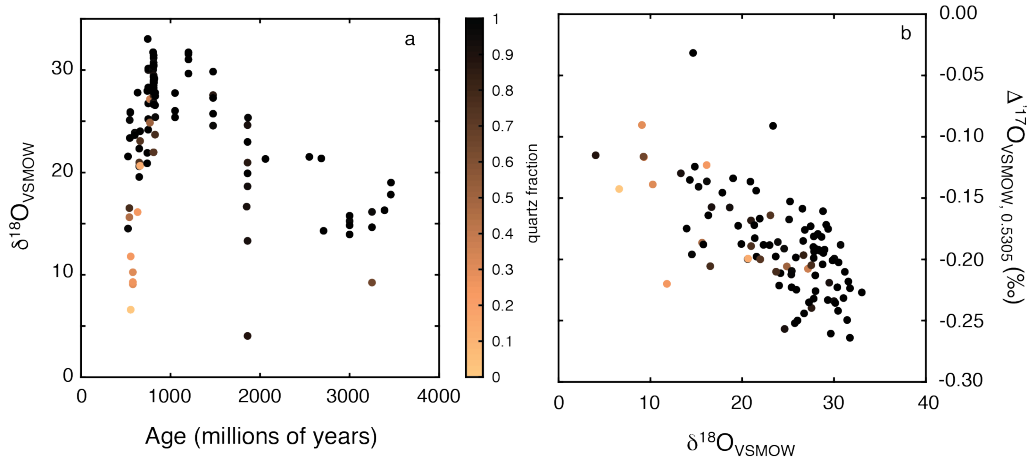


Figure 2: (a) The $\delta^{18}\text{O}$ as a function of time, with (b) $\Delta^{17}\text{O}$ as a function of $\delta^{18}\text{O}$ where individual data are colored according to the quartz fraction of the sample, as measured by XRD analysis. The scale bar for quartz fraction is included between the two frames, and only the black data (composed of more than 90% quartz) are used in subsequent analysis. Detailed mineralogy of each sample is listed in Table S2.

181 3.1. A stratigraphic test: the Fifteenmile Formation

182 Before we can investigate the differing models proposed to explain the
 183 information locked within the $\delta^{18}\text{O}$ of Precambrian chert, we must first test
 184 the scale at which chert is vulnerable to isotopic change. Put simply, if there

185 exists a wide compositional range within a given hand sample or across a well
 186 mixed paleo-basin, interpreting the same magnitude of signal across geologi-
 187 cal time would not be prudent. The first test, variability on the hand sample
 188 scale, was performed by comparing the isotopic composition of different nod-
 189 ules cut from the same sample. We ran this test 13 times, and the mean
 190 offset in $\Delta^{17}\text{O}$ is 0.004‰ , with a variance at 2σ for our analytical precision.
 191 The later of these tests, capturing how robust the ^{17}O in chert is across a
 192 single basin, is conducted on the Tonian aged Fifteenmile Formation. We
 193 present data from two parallel stratigraphic sections. The lion's share of the
 194 samples come from a 20 meter section of Mt. Slipper (section P1401, see
 195 [39]). The remainder of the data was generated on samples from the contem-
 196 poraneous beds within the Fifteenmile, roughly one kilometer away (section
 197 P1405, [39]). These data test for variability within a given stratigraphic sec-
 198 tion and across a paleo-basin. The mean $\Delta^{17}\text{O}$ from the P1401 section is
 199 $-0.200 \pm 0.022\text{‰}$, whereas section P1405 carried a mean of $-0.206 \pm 0.024\text{‰}$
 200 (Figure S3) . The two sections are thus statistically indistinguishable, but
 201 do carry some resolvable $\delta^{18}\text{O}$ variance. However, this variance is clearly not
 202 large enough to manifest in a resolvable, more mechanistic $\Delta^{17}\text{O}$ signal. For
 203 further context, the reproducibility of standards is near the statistics on these
 204 natural populations. Hence, the variability we observe within a single section
 205 is indistinguishable from the variability we expect based on our capacity of
 206 make precise $\Delta^{17}\text{O}$ measurements. This does not imply that the samples
 207 are unaltered, but simply that a cross section of samples at that geographic

scale can share a loosely similar life history. Indeed, there is resolvable $\delta^{18}\text{O}$ variability within the basin, however governing mass laws (or λ values) will not manifest an appreciable change in $\Delta^{17}\text{O}$ over such a small-scale $\delta^{18}\text{O}$ range. This would suggest that any alteration process must carry a λ between 0.5305 and 0.527 in order not to have generated an accompanying resolvable $\Delta^{17}\text{O}$. It is noteworthy that meteoric water falls a long a line of 0.528, a point considered more deeply below.

4. Discussion and Geologic scenarios

The new data generated through this study are in keeping with previous $\delta^{18}\text{O}$ measurements, these samples can be interpreted as a 'representative' sample suite with which to test pre-existing hypotheses in light of the new $\Delta^{17}\text{O}$ data. We do so in turn. We first individually consider changes in ocean temperature and the $\delta^{18}\text{O}$ composition of seawater itself, before ending with a discussion of diagenetic over-printing.

4.1. A change in global temperature

The new $\delta^{18}\text{O}$ measurements in this study could be explained by a progressive decrease in mean ocean temperature over the last 4 billion years. The decreasing temperature manifests as a change in the equilibrium isotope fractionation factor ($\alpha_{\text{chert-water}}$), offset relative to an ice-free ocean of constant composition (calculated as $\delta^{18}\text{O}$ of $\approx -1.2\text{‰}$, $\Delta^{17}\text{O}$ of $\approx -0.005\text{‰}$; and consistent with [23, 24]). In this scenario, the median $\delta^{18}\text{O}$ in the Archean

229 corresponds to a temperature of over 120°C, which subsequently evolves to a
 230 38°C Phanerozoic ocean. The physical interpretation of this temperature is
 231 itself controversial ([14, 46, 12]); however, an agnostic approach is to simply
 232 address the consistency of the $\Delta^{17}\text{O}$ prediction.

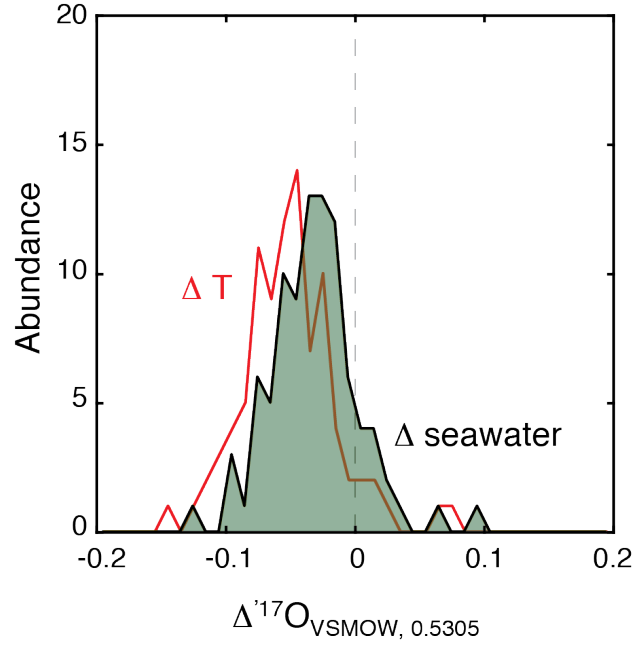


Figure 3: As noted in the text, changes in temperature and the composition of seawater through time make predictions for the associated oxygen isotope composition of seawater. Here, we present the residual, or mismatch, in $\Delta^{17}\text{O}$ between those model predictions and the data presented herein. The red line is the residual population for changing ocean temperatures, whereas the green shaded area is the residual for the evolving ocean $\delta^{18}\text{O}$. A perfect fit, for example, would have a distribution centered on a value of 0.00 ‰. The average value of the ocean $\delta^{18}\text{O}$ change residual is -0.034‰ and the average value of the temperature change residual is -0.054‰. Put differently, these models cannot, as formulated, satisfy the minor oxygen isotope data.

233 The existing $\delta^{18}\text{O}$ record corresponds to a unique temperature trend
 234 through geologic time, and these supposed temperatures in turn predict a
 235 corresponding $\Delta^{17}\text{O}$ composition assuming equilibrium fractionation [33].

236 The equilibrium λ , which controls the $\Delta^{17}\text{O}$, becomes smaller at lower tem-
 237 peratures, which ultimately produces a concave downward trend in $\Delta^{17}\text{O}$
 238 versus $\delta^{18}\text{O}$ (see Fig. S4). The degree of variability in $\Delta^{17}\text{O}$ does not al-
 239 low for a test on this predicted concavity, however the measured $\Delta^{17}\text{O}$ are
 240 consistently more negative than the predicted trend (on average, $\approx 0.05\text{‰}$:
 241 Figures 3 and S4). Based on this mismatch between predicted and measured
 242 compositions, the hypothesis that variability in the chert record is produced
 243 strictly by changes in the ocean temperature is not uniquely supported by
 244 the $\Delta^{17}\text{O}$ data.

245 It is noteworthy that most studies that advocate for elevated tempera-
 246 tures make the additional assumption that the heaviest $\delta^{18}\text{O}$ composition
 247 for each time-period, not the median value, reflects the primary composi-
 248 tion [15] - this allows for some degree of secondary alteration. Based on this
 249 interpretation, the Archean ocean would still be at 70-80°C, but no longer
 250 unrealistically hot. Unfortunately, this interpretive approach does not fur-
 251 ther minimize the mismatch between predicted and measured $\Delta^{17}\text{O}$ values.
 252 Changing the temperature prediction would shift the $\Delta^{17}\text{O}$ prediction along
 253 an equilibrium fractionation array, but it would not shift the array towards
 254 the field of measured compositions (see Fig. S4). The calculated equilibrium
 255 $\Delta^{17}\text{O}$ being offset from the measured data means, regardless of the temper-
 256 ature, a single equilibrium formation process will not capture the bulk of the
 257 geologic record. What is less convincing is the efficacy of the temperature
 258 model as a solution when placed relative to the other existing hypotheses.

259 *4.2. changing the composition of seawater*

260 Another possible explanation for the change in the $\delta^{18}\text{O}$ of SiO_2 through
261 the Precambrian (and by extension, throughout Earth history) is that the
262 actual $\delta^{18}\text{O}$ of seawater is evolving. Here, the equilibrium offset may be un-
263 changed (i.e. no change in surface temperatures), but the apparent effect in
264 chert drifts as a function of changing seawater composition. The $\delta^{18}\text{O}$ of sea-
265 water is set by interactions at both high and low temperature with basaltic
266 oceanic crust [47]. High-temperature exchange occurs at ridges and deep in
267 the ocean crust whereas low-temperature exchange happens during weather-
268 ing of continental crust and upper oceanic crust. This manifests isotopically
269 because high-temperature reactions are characterized by $^{18}\alpha \approx 1.002$ and low
270 temperature reactions are characterized by $^{18}\alpha = 1.020 - 1.045$ as a function
271 of temperature. Continental and oceanic crustal isotopic values are buffered
272 by recycling with a mantle, assumed to be infinitely large with constant
273 $\delta^{18}\text{O}$ composition. Modelling treatments [11] then allow the evolution of sea-
274 water by changing the dominant mode of the ocean-rock interaction from
275 low-temperature exchange in the Archean to high-temperature exchange in
276 the present.

277 Here we rebuild a popular model [11, 48] - designed to describe the $\delta^{18}\text{O}$ of
278 carbonate - with the eventual extension to chert ^{17}O to test this hypothesis.
279 This required the usage of a low-temperature $^{18}\alpha = 1.028$, which then enables
280 a test of the variable contribution from different weathering regimes. This
281 fractionation factor reflects the kaolinite - water equilibrium at 5 °C [49], and

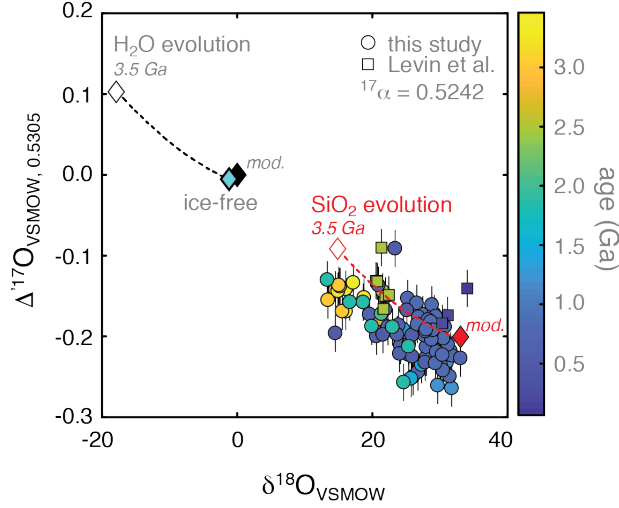


Figure 4: A plot of $\delta^{18}\text{O}$ against $\Delta^{17}\text{O}$. Measured chert compositions are shown, colored according to their age, with error bars reflecting the precision of the $\Delta^{17}\text{O}$ measurement. Error in $\delta^{18}\text{O}$ is smaller than the points. As in Figure 1, data from this study are circles while data from [25] are squares. The composition of VSMOW is 0 ‰ in both $\delta^{18}\text{O}$ and $\Delta^{17}\text{O}$ and is represented by the black diamond labeled 'mod.'. The ocean composition change hypothesis posits that seawater $\delta^{18}\text{O}$ increased through time, our geochemical model assigns a $\Delta^{17}\text{O}$ component to this evolution. The dashed black line shows the compositional change predicted by this model, from 3.5 Ga (white diamond) to the modern ice free ocean composition (cyan diamond). This is similar in directionality, but different in detail from other model predictions [23] based on differing formalism [47]. The dotted red line shows the parallel evolution of a predicted chert composition based on the commensurate change in the composition of seawater. The chert fractionation was calculated to best match the modern isotope offset between chert and seawater.

282 using a data-derived calibration [23], further allows for the calculation of an
 283 associated λ of 0.524. As our results are sensitive to this choice, a number
 284 of other scenarios are provided in the supplement (Figure S5). Moving for-
 285 ward, reproducing the entire chert $\delta^{18}\text{O}$ range requires more than 90% of the
 286 Archean ocean crust exchange to occur at low-temperature and more than
 287 90% of the Phanerozoic ocean crust exchange to occur at high temperature
 288 (Figure 3). The test comes with the assignment of ^{17}O fractionation factors

289 to each of the geologic pools and to each of the exchange fluxes based on the
 290 predicted temperature of that exchange ([31, 33, 28]; Fig. S4). This then
 291 predicts a $\Delta^{17}\text{O}$ composition of seawater in parallel to the $\delta^{18}\text{O}$ value. The
 292 evolving ocean oxygen isotope composition, as well as the chert composition
 293 of precipitated chert in equilibrium with that ocean, are shown in Figure
 294 4. Like with the temperature prediction discussed previously, the predicted
 295 chert trajectory parallels the triple isotope trend of the data, systematically
 296 offset towards more positive values (or leaving a negative residual, see Figure
 297 3). The isotopic mismatch of the changing seawater hypothesis is smaller
 298 than the changing temperature hypothesis, but still insufficient *by itself* as a
 299 mechanism for explaining the Precambrian chert record. It is also noteworthy
 300 that an unchanged seawater $\delta^{18}\text{O}$ composition is in keeping with Phanerozoic
 301 studies of carbonate clumped isotopes [17].

302 It is worth noting that the slope of the oxygen isotope trajectory of seawater
 303 in $\delta^{17}\text{O}$ - $\delta^{18}\text{O}$ space is controlled primarily by the λ of the low-temperature
 304 exchange processes. If low-temperature ocean-rock exchange is driven using
 305 a larger λ , closer to the high-temperature end-member of 0.5305, then there
 306 would be less contrast in $\Delta^{17}\text{O}$ between the high- and low-temperature ex-
 307 change. The oceans $\delta^{18}\text{O}$ could then evolve without changing $\Delta^{17}\text{O}$, thereby
 308 causing the chert trajectory to intercept the bulk of our measurements. Due
 309 to the temperature dependence of both α and λ it is impossible however
 310 to independently change one without affecting the other, and using a larger
 311 value for λ would require a correspondingly smaller value of α , which would

312 make it impossible to reproduce the $\delta^{18}\text{O}$ record. This sensitivity is captured
313 in Figure S5.

314 4.3. diagenetic alteration

315 The previous hypotheses forwarded to explain the isotopic composition
316 of Precambrian chert rely on the capacity of SiO_2 to retain a primary de-
317 positional signal despite potential later interactions with geological fluids.
318 In fact, in the previously described case where only the heaviest $\delta^{18}\text{O}$ are
319 interpreted for an extracted temperature record, some degree of diagenetic
320 vulnerability is inferred. Great efforts have been taken (cf. [50]) to under-
321 stand the degree to which the geochemical and isotopic composition of rocks
322 and minerals have been altered through time. The oxygen isotope compo-
323 sition of geologic samples are particularly susceptible to diagenetic resetting
324 given the water-rich, high oxygen content (water at 89%) of alteration fluids.
325 This case becomes even more exacerbated when thinking about a largely per-
326 itidal facies, which would be subjected in even the shortest term to changes
327 in alteration fluid as a function of sea level change. This proposed diagenetic
328 alteration could come anytime between lithification and the field season the
329 sample suite was collected. A simple stochastic exercise demonstrates such
330 a phenomenon. In a purely synthetic sense, if alteration is random and al-
331 lowed to occur at variable (random) magnitudes and rate through time, a
332 time-dependent record (Figure 5) is predicted. Importantly, this exercise is
333 devoid of geological observables, but demonstrates alteration-potential and

334 as meant as simply an example.

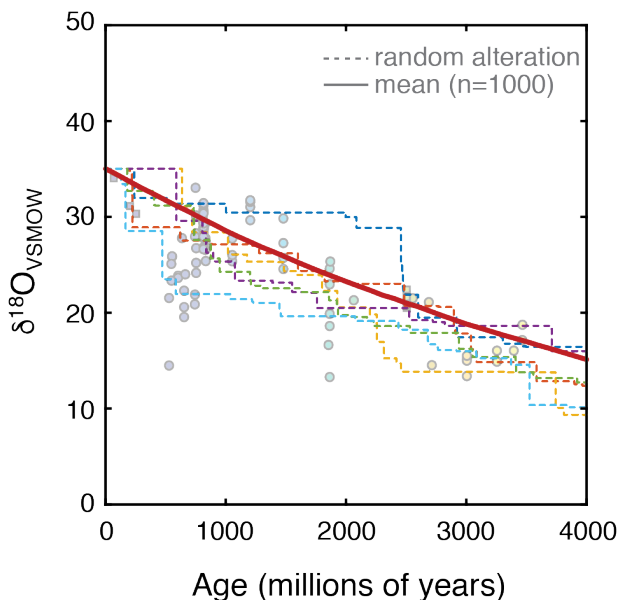


Figure 5: Here we present the results of a random alteration model designed to test the capacity of diagenesis to reproduce the chert $\delta^{18}\text{O}$ record. Model chert precipitated with an initial $\delta^{18}\text{O}$ of 35 ‰ (y-axis), then, with random intervals and magnitude, become altered over time (x-axis). In gray is the $\delta^{18}\text{O}$ data from this study. Colored lines reflect six examples of individual model simulations, and the heavy red line is the mean of 1000 simulations. This simply demonstrates that random alteration, more likely as the age of the geological unit increases, can produce the sort of first order signal preserved in the chert (and other oxygen bearing phases) record(s).

335 Diagenetic alteration generally carries a non-unique, rather than specific
 336 prediction for the isotopic composition of chert. The most basic approach is
 337 first adopting the null hypothesis that all SiO_2 precipitated with an isotopic
 338 composition comparable to today, and any deviation from this composition
 339 is the result of alteration. From here, three primary variables control the
 340 ultimate composition of chert: the temperature and isotopic composition of
 341 the secondary fluid, and the degree of alteration (water to rock ratio). Not

surprisingly, each variable can be tuned to reproduce the geologic record of $\delta^{18}\text{O}$ and $\Delta^{17}\text{O}$.

Like $\delta^{18}\text{O}$, diagenesis carries a suite of predictions for the associated $\Delta^{17}\text{O}$. Here, mixing between two isotopic compositions produces a concave upward array, distinct from equilibrium fractionation lines. The curvature becomes more pronounced as the two end-members become more isotopically different. Due to the concavity, mixing between a modern-like initial chert composition and SiO_2 reset by interactions with higher-temperature fluids can easily satisfy the $\delta^{18}\text{O}$ and $\Delta^{17}\text{O}$ of Precambrian chert. As discussed more below, this is in part because of the flexibility in parameters noted above, which allow the data to essentially be fit, minimizing the residual between model predictions and the data.

The model fit serves to inform the mechanisms acting on the original isotopic composition of SiO_2 . It is apparent that alteration with a fluid carrying a modern seawater-like composition does not best fit the Precambrian data. Early diagenesis at some stage in the life-history of the sedimentary unit may indeed be seawater-buffered, but later diagenesis can be driven by fluids sourced from meteoric water with highly variable compositions [51]. Alteration with meteoric water has two important consequences in the context of this hypothesis. First, this fluid is lighter in $\delta^{18}\text{O}$ than seawater, thereby forming a larger mixing curve with the primary chert that subsequently results in more negative $\Delta^{17}\text{O}$ compositions. Second, meteoric water has a range of compositions rather than a unique value, therefore producing a field

365 of possible solutions rather than a single unique solution. The single mixing
 366 line which minimizes the residual between model and data, shown in Figure
 367 6, defines the initial chert to be precipitated at 30°C and have been altered by
 368 a fluid (likely groundwater) groundwater with a $\delta^{18}\text{O}$ composition of -16.5‰.
 369 Importantly, resampling allows meteoric water to freely vary from -25 - 0 ‰,
 370 and the -16.5 ‰ is simply the best *bulk* fit to the entire dataset. These best-
 371 fit values are reasonable on the modern Earth, and this solution supports
 372 a uniformitarian perspective of Earth history whereby the temperature and
 373 isotopic composition of the ocean has remained relatively stable.

374 The possibility of alteration is not a bi-modal distinction, but the sug-
 375 gestion that more than a primary depositional condition is recording in the
 376 composition of the targeted chert. Admittedly, this hypothesis suggests that
 377 some primary geochemical information is irrevocably lost. However, even
 378 the most altered Archean samples only experienced a W-R ratio of 1 (here
 379 we use a classic definition of water:rock, and is discussed in detail below),
 380 and thus the majority of the signal is still primary. While it will be difficult
 381 to identify a unique initial composition for any individual chert, especially
 382 without a tightly constrained composition of alteration fluid, a substantial
 383 fraction of the signal remains.

384 4.4. a multivariate approach

385 Part of the difficulty in distinguishing between the three primary hypothe-
 386 ses surrounding the long-term change in $\delta^{18}\text{O}$ is that they are not mutually

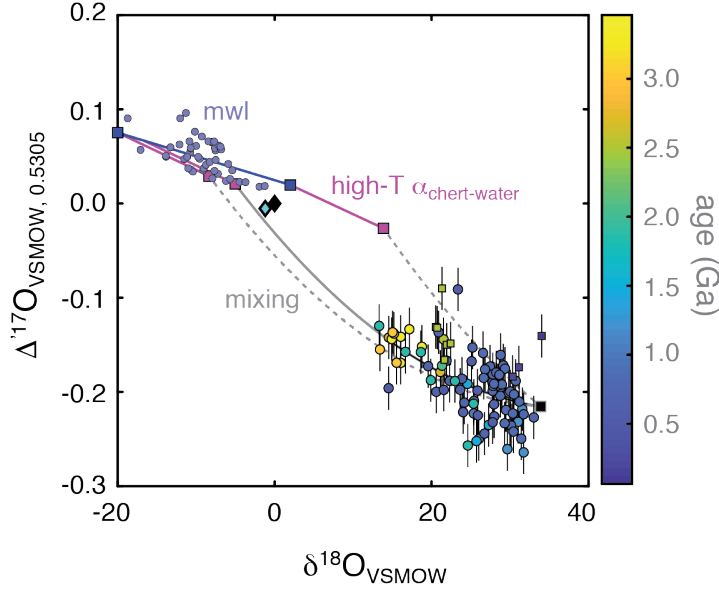


Figure 6: Here we show an alteration model where a primary chert composition precipitated from an ice free ocean, shown as the blue diamond, is altered at high temperature by meteoric water. Meteoric water compositions and blue best fit line (mw: meteoric water line) from [52]. The offset from this line, set in magenta, is the high-temperature equilibrium fractionation factor for the new, now modified SiO_2 composition. This offset is defined as the equilibrium prediction at 200°C . The dotted grey lines show the mixing (alteration) line between the primary chert composition and various meteoric water compositions. The black line is the mixing line that minimizes the residual between the model prediction and the measured data (colored data points). The best fit for the entire dataset is defined by a water value of -16.5‰ , alteration at 200°C , and a primary precipitation temperature of 30°C , but varying these parameters would allow for the flexibility to fit the outlying data.

387 exclusive. All three mechanisms could, in conjunction, influence the $\delta^{18}\text{O}$ and
 388 $\Delta^{17}\text{O}$ composition of the sampled chert. Above, we analyzed the hypothe-
 389 ses in isolation, showing how the mechanisms would be expressed in $\Delta^{17}\text{O}$
 390 - this suggested that diagenetic alteration provides the most statistically ro-
 391 bust single answer. This comes as little surprise, given the flexibility (in
 392 parameter space) associated with that solution. Moving forward, however,

we can evaluate the relative contribution of these different environmental solutions/parameters in parallel.

Here we provide a synthetic resampling routine that allows all of the features of interest to vary within reasonable bounds. The variables, shown in Table S3, include 1) the degree of ocean evolution, 2) the degree of glacial or evaporative seawater distillation, 3) the temperature of precipitation, 4) the temperature of the alteration fluid, 5) the composition of the alteration fluid, and 6) the degree of alteration (water to rock ratio). The final chert composition is calculated using the equation:

$$\delta^{1x}O_{c-altered} = \frac{W/R * \left((\alpha_{f-c,high-T} - 1) * 1000 + \delta^{1x}O_{f,low-T} \right) + \delta^{1x}O_{c,lowT}}{W/R + 1} \quad (5)$$

where W/R is the water to rock ratio, the superscript 1x represents either ^{18}O or ^{17}O , the subscript f represents the alteration fluid, high-T and low-T relate to temperature, and the subscript c represents the chert. This style of resampling analysis provides information about both what variables are most likely to control the output isotopic composition and also over what range of values each variable is most likely to cover.

In this approach, the analysis uniformly generates random values for the six primary variables and derives a predicted chert $\delta^{18}\text{O}$ and $\Delta^{17}\text{O}$ composition for that combination of variable inputs. If the calculated synthetic chert composition corresponds to an actual measured chert composition in the

412 dataset to within 0.1‰ for $\delta^{18}\text{O}$ and 0.01‰ for $\Delta^{17}\text{O}$ (conservative bounds,
 413 given our uncertainty), the values of the six variables are saved in association
 414 with that chert sample. This generates a curated suite of variable sets, or
 415 mathematically viable solutions for each individual data point. In fact, each
 416 datum is described by many sets of the six variables. As with a Monte Carlo
 417 resampling regime, the curated results will carry a distribution that reflects
 418 the specificity or sensitivity of that variable to the overall chert composition.
 419 The superposition of these individual datasets captures the average envi-
 420 ronmental conditions required to reproduce the Precambrian triple oxygen
 421 isotope composition of chert. This analysis was run $5 \cdot 10^7$ times, with 3.5%
 422 of the random solutions satisfying the composition of at least one measured
 423 value. The full, uncurated field of solutions is presented in Figure 7, with
 424 our measured data plotted on top of it.

425 The synthetic resampling routine generated a field of interesting, and in-
 426 terpretable information. Figure 8 provides a probability density function for
 427 each of the parameters tested. Let us first note how to interpret these fields.
 428 The value in the Y axis (the density function) is the accounting for how
 429 many solutions existed for a given x axis value. Here, solutions are those
 430 sets of model inputs that can satisfy any of the given chert compositional
 431 measurements. In essence then, the histograms in Figure 8 are recast and
 432 summed versions of heat maps like that presented in Figure 7. In cases where
 433 the histogram carries structure, there is a specificity within that parameter
 434 space necessary to account for the observed chert compositions. In the cases

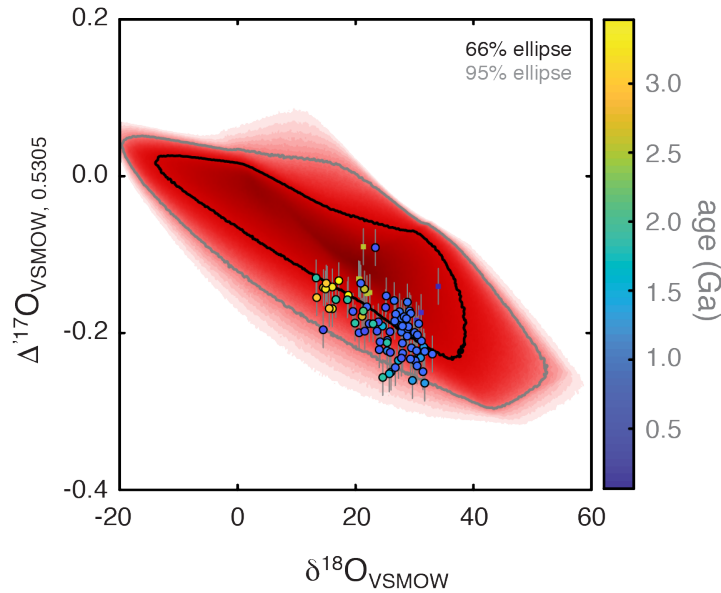


Figure 7: A plot of $\delta^{18}\text{O}$ vs $\Delta^{17}\text{O}$ showing the complete probabilistic results of the stochastic model, in red, compared to the measured chert isotope data. The shade of red reflects the density of model solutions for that unique composition - darker indicates that an increased fraction of the random inputs produced chert with that composition. The tested variables and values thereof are presented in Table S3. The grey and black envelopes show the position of 95% and 66% of the results respectively. The centroid of the synthetic results plots above the measured data because, as established in the main text, temperature and ocean change driven fractionations produce $\Delta^{17}\text{O}$ values more positive than the measured data.

where little structure is present (i.e. a flat line), that variable - according to this analysis - does not carry much sensitivity or likelihood of contributing to the overall preserved chert values. Of the histograms shown, some directly correspond to the three primary hypotheses discussed above. First, Figure 8a, in blue, shows the predicted equilibrium precipitation temperature, which in our model corresponds to contemporaneous ocean temperatures. Here the suggestion is for an equitable, modern-like climate where the median seawater temperature varies around about 23 °C. Few solutions recorded elevated

443 primary surface ocean temperatures. Next, and as captured in Figure 8b,
 444 in red, we evaluate the chances that changes in the $\delta^{18}\text{O}$ of seawater itself
 445 are actually driving the observations captured in the chert record. Values
 446 of zero reflect a constant ocean $\delta^{18}\text{O}$ composition through time, whereas a
 447 value of 1 reflects an ocean that evolves parallel to the chert data. Nega-
 448 tive values scale similarly, with the prediction of decreasing $\delta^{18}\text{O}$ of seawater
 449 through time. Interpreting this variable brings with it more ambiguity, as
 450 the data can all be satisfied without a change in seawater $\delta^{18}\text{O}$, however
 451 some moderate change to low:high temperature alteration does describe the
 452 median solution. As alteration hypotheses regarding the balance of high and
 453 low temperature weathering regimes through time are rooted in geophysical
 454 arguments related to heat loss, the likelihood of an intermediate state or
 455 weathering balance/solution should be evaluated on those grounds¹. Small
 456 changes in seawater $\delta^{18}\text{O}$ and $\Delta^{17}\text{O}$ can also be accommodated with variable
 457 ice volume, captured in Figure 8f, but the data is better fit with a modest
 458 glacial fraction.

459 Finally, Figure 8c-e in green captures the principle components of diage-

¹With respect to seawater $\delta^{18}\text{O}$ evolution through time (Figure 8b), the analysis has seemingly little dependence on this constraint. However, to further probe the model of [11], the model was run twice, with the glacial fraction defined as 0 and the ocean evolution defined as either 1 or 0. The ocean with evolving isotopic composition had only 77% as many model solutions as the isotopically "constant" ocean. Additionally, the evolving ocean model did not produce solutions for 10 of the measured samples, whereas the "constant" ocean carried solutions for all but 4 measured samples. These results further suggest that an isotopically evolving ocean can adequately reproduce the measured data, but an ocean of constant composition is better statistically supported.

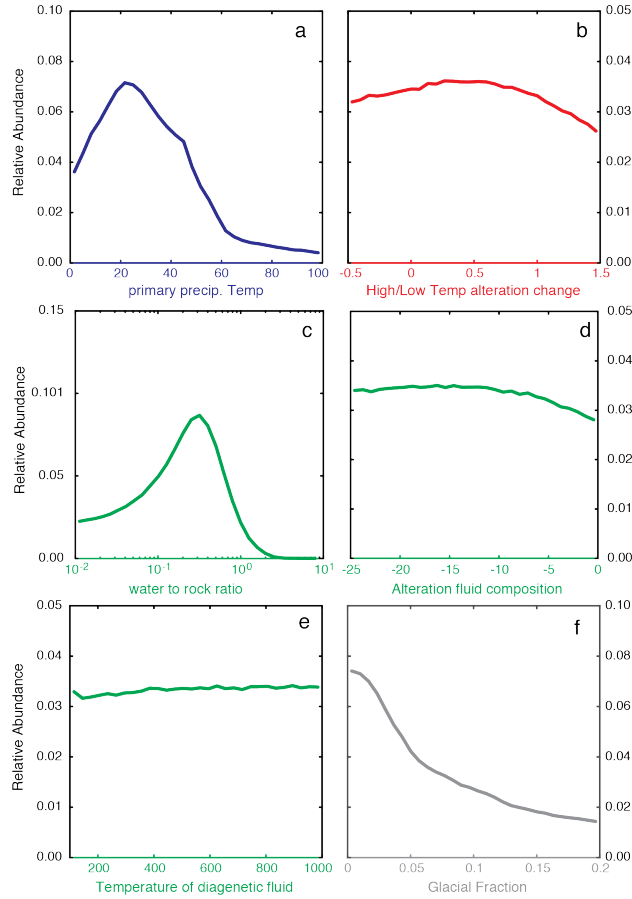


Figure 8: Monte Carlo model results for each tested variable. In each plot the x axis shows the allowed range of variation for the random input variable, the y axis shows the relative abundance of that value among inputs that reproduced measured data. Each histogram is composed of the compiled fits for all measured data points. Line colors represent the primary hypothesis each variable tests, blue for the warm early ocean hypothesis, red for the ocean $\delta^{18}\text{O}$ evolution hypothesis, green for the diagenesis hypothesis, and grey for glaciation. Although we do not discuss the role of glacial ice, we include it for the sake of being complete. The water to rock ratio shown in c is displayed with a logarithmic x axis, but like with the other variables, the inputs are generated such that each value in this plotted space is equally probable.

460 nesis. For instance, we present predictions for water to rock ratio, alteration
461 fluid composition and temperature. The W-R prediction suggests that, while
462 some chert can be explained as relatively unaltered - i.e. W-R ratio below
463 0.1 - the large majority require diagenetic resetting. Further, the predictions
464 here is that alteration occurred at higher temperatures (where equilibrium
465 fractionation factors vary less per unit temperature) with fluids of a meteoric-
466 like composition - none of which is geologically unreasonable. There is an
467 important linkage here between the temperature predictions and geologic ob-
468 servables. We define high-temperature alteration as elevated over seawater
469 temperatures, but still could be as low as a couple hundred degrees (or less).
470 Thus, scaling to something like metamorphic grade is challenging. Finally,
471 there is also more information to potentially gain as narrower time domains
472 are treated independently, as opposed to approaching the dataset as a whole.
473 Although interesting, these results are in keeping with the overall story for-
474 ward from the analysis of the entire dataset (Figure S6).

475 Simply presenting a histogram of compiled W-R ratios as in Figure 8c is
476 not sufficient to establish that variable alteration drives the classic chert $\delta^{18}\text{O}$
477 record. We must show that the progressively lighter $\delta^{18}\text{O}$ compositions are
478 matched in the model with progressively more alteration. To do this we found
479 the median predicted W-R ratio for each datapoint in our resampling model,
480 the value that is most representative of the degree of alteration, and plotted
481 it against the measured $\delta^{18}\text{O}$ (Figure 9). No corresponding relationship exists
482 between $\delta^{18}\text{O}$ and the modeled precipitation temperature (Figure S7). This

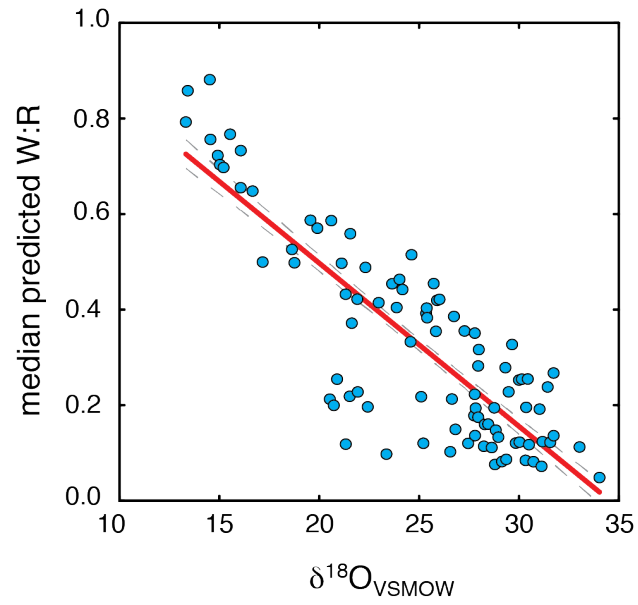


Figure 9: The measured $\delta^{18}\text{O}$ of the chert (x-axis) against the best fit of the modeled Monte Carlo W-R ratio (y-axis) for each chert measurement. Red line shows the linear best fit and suggests that different degrees of alteration produce the observed variation in $\delta^{18}\text{O}$.

483 result shows that the $\delta^{18}\text{O}$ and $\Delta^{17}\text{O}$ records in chert have an important
484 diagenetic component, a conclusion that could not be reached with $\delta^{18}\text{O}$
485 record alone.

486 5. Conclusion

487 The oxygen isotopic composition of Precambrian chert has long stood
488 as one of the most robust empirical records of Earth surface change, but
489 interpretations of this record are mired in controversy. Complicating these
490 interpretations is the observation of similar temporal patterns in the oxygen
491 isotope composition of Precambrian phosphate, iron oxide, carbonate miner-
492 als, as well as bulk shale. Further, arguments based on Si [53] and D/H [14]
493 isotopes within chert must be accommodated by any prescribed life history
494 of this material required for the O isotopes.

495 Here we provide another isotopic axis along which to test these various
496 hypotheses - the inclusion of ^{17}O . The triple oxygen isotope data of Precam-
497 brian chert places more specific requirements for various models employed to
498 describe the composition of chert. For instance, through these measurements
499 and associated models we show that changes in the isotopic composition of
500 seawater, and/or elevated Archean surface temperatures are less likely the
501 singular solution for the $\delta^{18}\text{O}$ record - differential diagenetic alteration has
502 almost certainly played an important role. This result broadly corresponds
503 to previous work interpreting $\Delta^{17}\text{O}$ in chert, but is in contrast to the shale
504 and iron oxide $\delta^{18}\text{O}$ records that suggest a change in seawater crust interac-

505 tions [23, 22, 21]. We do note that our analysis can allow for some variance
506 in seawater composition, on the scale suggested elsewhere [24, 54], despite it
507 not statistically being the lone cause. For our data, the most parsimonious
508 solution calls upon equitable surface temperatures, and secondary fluids that
509 look very meteoric in composition ($\approx -15\text{‰}$) at common subsurface tem-
510 peratures of a couple hundred degrees. This implies that some, but not
511 necessarily all original information is lost from these phases.

512 These predictions are consistent with existing Si and D/H isotope data.
513 In the case of Si, there is no correlation (at the 2σ level) in the 23 cases where
514 oxygen and Si data are available on the same sample (Figure S8). This is
515 to be expected, as the silicic acid content of alteration fluids would favor the
516 resetting of oxygen long before similar changes were witnessed in silicon. The
517 hydrogen isotopes record in chert has been used to argue for low Archean
518 ocean temperatures [14] - a prediction from this work as well - but arrived
519 at such a conclusion through invoking a temporal change in ocean $\delta^{18}\text{O}$. It is
520 possible that the δD of chert, not being a structural component of the quartz
521 mineral, preserves a different environmental window than that of oxygen.

522 If, as we argue, the oxygen isotopic composition of Precambrian chert
523 carries a significant component of alteration, then the adjoined prediction
524 is that phosphate, iron oxide, carbonate, and bulk siliciclastics experienced
525 similar histories. These parallel records show a shift in $\delta^{18}\text{O}$ of comparable
526 magnitude over the same time period, but the different oxygen-bearing phases
527 carry differing susceptibilities to alteration. Further work comparing the

thermodynamic properties of adjacent mineral phases, perhaps using ^{17}O in these actual minerals, or more generally using the model results presented above, will serve to help quantify these co-occurring changes.

In summary, the $\Delta^{17}\text{O}$ record of Precambrian chert is not solely a primary depositional signal. The question remains of how to see through this alteration to a primary composition. Of course, this model (and statistics therein) allow for some change in the $\delta^{18}\text{O}$ of seawater, but are significantly less in keeping with major changes in surface ocean temperatures through time. This contributes to the long-standing debate in the geologic community about the origin of this signal and demonstrates the utility of mass-dependent, multiple isotope systematics to Earth history questions.

- 539 [1] H. C. Urey, The thermodynamic properties of isotopic substances, Jour-
540 nal of the Chemical Society (Resumed) (1947) 562–581.
- 541 [2] J. Zachos, M. Pagani, L. Sloan, E. Thomas, K. Billups, Trends, rhythms,
542 and aberrations in global climate 65 ma to present, *Science* 292 (2001)
543 686–693.
- 544 [3] N. J. Shackleton, Paleotemperature history of the cenozoic and the
545 initiation of antarctic glaciation: oxygen and carbon isotope analyses in
546 dsdp sites 277, 279, and 281, Initial Reports of Deep Sea Drilling Project
547 29 (1975) 743–756.
- 548 [4] J. L. Banner, G. N. Hanson, Calculation of simultaneous isotopic and
549 trace element variations during water-rock interaction with applications
550 to carbonate diagenesis, *Geochimica et Cosmochimica Acta* 54 (1990)
551 3123–3137.
- 552 [5] M. Schobben, C. V. Ullmann, L. Leda, D. Korn, U. Struck, W. U.
553 Reimold, A. Ghaderi, T. J. Algeo, C. Korte, Discerning primary versus
554 diagenetic signals in carbonate carbon and oxygen isotope records: An
555 example from the permian–triassic boundary of iran, *Chemical Geology*
556 422 (2016) 94–107.
- 557 [6] L. P. Knauth, Temperature and salinity history of the precambrian
558 ocean: implications for the course of microbial evolution (2005) 53–69.

- 559 [7] L. P. Knauth, S. Epstein, Hydrogen and oxygen isotope ratios in nodular
560 and bedded cherts, *Geochimica et Cosmochimica Acta* 40 (1976) 1095–
561 1108.
- 562 [8] J. Marin, M. Chaussidon, F. Robert, Microscale oxygen isotope vari-
563 ations in 1.9 ga gunflint cherts: assessments of diagenesis effects and
564 implications for oceanic paleotemperature reconstructions, *Geochimica*
565 *et Cosmochimica Acta* 74 (2010) 116–130.
- 566 [9] P. Jean-Baptiste, J. Charlou, M. Stievenard, Oxygen isotope study
567 of mid-ocean ridge hydrothermal fluids: Implication for the oxygen-18
568 budget of the oceans, *Geochimica et Cosmochimica Acta* 61 (1997)
569 2669–2677.
- 570 [10] J. F. Kasting, M. T. Howard, K. Wallmann, J. Veizer, G. Shields,
571 J. Jaffrés, Paleoclimates, ocean depth, and the oxygen isotopic com-
572 position of seawater, *Earth and Planetary Science Letters* 252 (2006)
573 82–93.
- 574 [11] J. B. Jaffrés, G. A. Shields, K. Wallmann, The oxygen isotope evolution
575 of seawater: A critical review of a long-standing controversy and an
576 improved geological water cycle model for the past 3.4 billion years,
577 *Earth-Science Reviews* 83 (2007) 83–122.
- 578 [12] J. Veizer, A. Prokoph, Temperatures and oxygen isotopic composition
579 of phanerozoic oceans, *Earth-Science Reviews* 146 (2015) 92–104.

- 580 [13] E. T. Degens, S. Epstein, Relationship between $\delta^{18}\text{O}/\delta^{16}\text{O}$ ratios in co-
581 existing carbonates, cherts, and diatomites, AAPG Bulletin 46 (1962)
582 534–542.
- 583 [14] M. Hren, M. Tice, C. Chamberlain, Oxygen and hydrogen isotope evi-
584 dence for a temperate climate 3.42 billion years ago, Nature 462 (2009)
585 205.
- 586 [15] F. Robert, M. Chaussidon, A palaeotemperature curve for the precam-
587 brian oceans based on silicon isotopes in cherts, Nature 443 (2006) 969.
- 588 [16] R. E. Blake, S. J. Chang, A. Lepland, Phosphate oxygen isotopic evi-
589 dence for a temperate and biologically active archaean ocean, Nature
590 464 (2010) 1029.
- 591 [17] G. A. Henkes, B. H. Passey, E. L. Grossman, B. J. Shenton, T. E.
592 Yancey, A. Pérez-Huerta, Temperature evolution and the oxygen iso-
593 tope composition of phanerozoic oceans from carbonate clumped isotope
594 thermometry, Earth and Planetary Science Letters 490 (2018) 40–50.
- 595 [18] P. Ghosh, J. Adkins, H. Affek, B. Balta, W. Guo, E. A. Schauble,
596 D. Schrag, J. M. Eiler, $\delta^{13}\text{C}$ – $\delta^{18}\text{O}$ bonds in carbonate minerals: a new
597 kind of paleothermometer, Geochimica et Cosmochimica Acta 70 (2006)
598 1439–1456.
- 599 [19] J. M. Eiler, clumped-isotope geochemistry the study of naturally-

- 600 occurring, multiply-substituted isotopologues, *Earth and Planetary Sci-*
601 *ence Letters* 262 (2007) 309–327.
- 602 [20] K. J. Dennis, D. P. Schrag, Clumped isotope thermometry of car-
603 bonatites as an indicator of diagenetic alteration, *Geochimica et Cos-*
604 *mochimica Acta* 74 (2010) 4110–4122.
- 605 [21] N. Galili, A. Shemesh, R. Yam, I. Brailovsky, M. Sela-Adler, E. M.
606 Schuster, C. Collom, A. Bekker, N. Planavsky, F. A. Macdonald, et al.,
607 The geologic history of seawater oxygen isotopes from marine iron ox-
608 ides, *Science* 365 (2019) 469–473.
- 609 [22] I. Bindeman, D. Zakharov, J. Palandri, N. D. Greber, N. Dauphas,
610 G. Retallack, A. Hofmann, J. Lackey, A. Bekker, Rapid emergence of
611 subaerial landmasses and onset of a modern hydrologic cycle 2.5 billion
612 years ago, *Nature* 557 (2018) 545.
- 613 [23] S. Sengupta, A. Pack, Triple oxygen isotope mass balance for the earth’s
614 oceans with application to Archean cherts, *Chemical Geology* 495 (2018)
615 18–26.
- 616 [24] D. Zakharov, I. Bindeman, R. Tanaka, G. Friðleifsson, M. Reed,
617 R. Hampton, Triple oxygen isotope systematics as a tracer of fluids in
618 the crust: A study from modern geothermal systems of Iceland, *Chem-*
619 *ical Geology* 530 (2019) 119312.

- 620 [25] N. E. Levin, T. D. Raub, N. Dauphas, J. M. Eiler, Triple oxygen isotope
621 variations in sedimentary rocks, *Geochimica et Cosmochimica Acta* 139
622 (2014) 173–189.
- 623 [26] H. Craig, Isotopic standards for carbon and oxygen and correction fac-
624 tors for mass-spectrometric analysis of carbon dioxide, *Geochimica et*
625 *cosmochimica acta* 12 (1957) 133–149.
- 626 [27] E. D. Young, A. Galy, H. Nagahara, Kinetic and equilibrium mass-
627 dependent isotope fractionation laws in nature and their geochemical
628 and cosmochemical significance, *Geochimica et Cosmochimica Acta* 66
629 (2002) 1095–1104.
- 630 [28] X. Cao, Y. Liu, Equilibrium mass-dependent fractionation relationships
631 for triple oxygen isotopes, *Geochimica et Cosmochimica Acta* 75 (2011)
632 7435–7445.
- 633 [29] I. Ahn, J. I. Lee, M. Kusakabe, B.-G. Choi, Oxygen isotope measure-
634 ments of terrestrial silicates using a co 2-laser brf 5 fluorination technique
635 and the slope of terrestrial fractionation line, *Geosciences Journal* 16
636 (2012) 7–16.
- 637 [30] R. Tanaka, E. Nakamura, Determination of ^{17}O -excess of terrestrial
638 silicate/oxide minerals with respect to vienna standard mean ocean wa-
639 ter (vsmow), *Rapid Communications in Mass Spectrometry* 27 (2013)
640 285–297.

- 641 [31] A. Pack, D. Herwartz, The triple oxygen isotope composition of the
642 earth mantle and understanding $\delta^{17}\text{O}$ variations in terrestrial rocks and
643 minerals, *Earth and Planetary Science Letters* 390 (2014) 138–145.
- 644 [32] E. D. Young, L. Y. Yeung, I. E. Kohl, On the $\delta^{17}\text{O}$ budget of atmospheric
645 O_2 , *Geochimica et Cosmochimica Acta* 135 (2014) 102–125.
- 646 [33] Z. Sharp, J. Gibbons, O. Maltsev, V. Atudorei, A. Pack, S. Sengupta,
647 E. Shock, L. Knauth, A calibration of the triple oxygen isotope frac-
648 tionation in the $\text{SiO}_2\text{--H}_2\text{O}$ system and applications to natural samples,
649 *Geochimica et Cosmochimica Acta* 186 (2016) 105–119.
- 650 [34] E. D. Young, I. E. Kohl, P. H. Warren, D. C. Rubie, S. A. Jacobson,
651 A. Morbidelli, Oxygen isotopic evidence for vigorous mixing during the
652 moon-forming giant impact, *Science* 351 (2016) 493–496.
- 653 [35] B. R. Cowie, D. T. Johnston, High-precision measurement and standard
654 calibration of triple oxygen isotopic compositions ($\delta^{18}\text{O}$, $\delta^{17}\text{O}$) of sulfate
655 by F_2 laser fluorination, *Chemical Geology* 440 (2016) 50–59.
- 656 [36] R. Siever, The silica cycle in the precambrian, *Geochimica et Cos-*
657 *mochimica Acta* 56 (1992) 3265–3272.
- 658 [37] A. Knoll, Exceptional preservation of photosynthetic organisms in sili-
659 cified carbonates and silicified peats, *Philosophical Transactions of the*
660 *Royal Society of London. B, Biological Sciences* 311 (1985) 111–122.

- 661 [38] R. G. Maliva, A. H. Knoll, B. M. Simonson, Secular change in the pre-
662 cambrian silica cycle: insights from chert petrology, Geological Society
663 of America Bulletin 117 (2005) 835–845.
- 664 [39] P. A. Cohen, J. V. Strauss, A. D. Rooney, M. Sharma, N. Tosca, Con-
665 trolled hydroxyapatite biomineralization in an ~ 810 million-year-old uni-
666 cellular eukaryote, Science advances 3 (2017) e1700095.
- 667 [40] N. J. Tosca, S. Guggenheim, P. K. Pufahl, An authigenic origin for pre-
668 cambrian greenalite: Implications for iron formation and the chemistry
669 of ancient seawater, Bulletin 128 (2016) 511–530.
- 670 [41] W. W. Fischer, A. H. Knoll, An iron shuttle for deepwater silica in late
671 archean and early paleoproterozoic iron formation, Geological Society
672 of America Bulletin 121 (2009) 222–235.
- 673 [42] A. Bekker, J. F. Slack, N. Planavsky, B. Krapez, A. Hofmann, K. O.
674 Konhauser, O. J. Rouxel, Iron formation: the sedimentary product of
675 a complex interplay among mantle, tectonic, oceanic, and biospheric
676 processes, Economic Geology 105 (2010) 467–508.
- 677 [43] B. Rasmussen, J. R. Muhling, W. W. Fischer, Evidence from laminated
678 chert in banded iron formations for deposition by gravitational settling
679 of iron-silicate muds, Geology 47 (2019) 167–170.
- 680 [44] J. Marin-Carbone, F. Robert, M. Chaussidon, The silicon and oxygen

- isotope compositions of precambrian cherts: A record of oceanic paleo-
temperatures?, *Precambrian Research* 247 (2014) 223–234.
- [45] H. Bao, M. H. Thiemens, Generation of O_2 from BaSO_4 using a CO_2 -
laser fluorination system for simultaneous analysis of $\delta^{18}\text{O}$ and $\delta^{17}\text{O}$,
Analytical chemistry 72 (2000) 4029–4032.
- [46] R. Tartèse, M. Chaussidon, A. Gurenko, F. Delarue, F. Robert, Warm
archean oceans reconstructed from oxygen isotope composition of early-
life remnants, *Geochemical Perspectives Letters* 3 (2017) 55–65.
- [47] K. Muehlenbachs, R. Clayton, Oxygen isotope composition of the
oceanic crust and its bearing on seawater, *Journal of Geophysical Re-
search* 81 (1976) 4365–4369.
- [48] K. Wallmann, The geological water cycle and the evolution of marine
 $\delta^{18}\text{O}$ values, *Geochimica et Cosmochimica Acta* 65 (2001) 2469–2485.
- [49] S. Sheppard, H. Gilg, Stable isotope geochemistry of clay minerals, *Clay
Minerals* 31 (1996) 1–24.
- [50] L. A. Derry, A burial diagenesis origin for the ediacaran shuram–wonoka
carbon isotope anomaly, *Earth and Planetary Science Letters* 294 (2010)
152–162.
- [51] S. Li, N. E. Levin, L. A. Chesson, Continental scale variation in ^{17}O -
excess of meteoric waters in the united states, *Geochimica et Cos-
mochimica Acta* 164 (2015) 110–126.

- 702 [52] B. Luz, E. Barkan, Variations of $^{17}\text{O}/^{16}\text{O}$ and $^{18}\text{O}/^{16}\text{O}$ in meteoric
703 waters, *Geochimica et Cosmochimica Acta* 74 (2010) 6276–6286.
- 704 [53] R. Chakrabarti, A. H. Knoll, S. B. Jacobsen, W. W. Fischer, Si isotope
705 variability in proterozoic cherts, *Geochimica et Cosmochimica Acta* 91
706 (2012) 187–201.
- 707 [54] B. Johnson, B. Wing, Archean seawater, *Geology* (2020).
- 708 [55] F. A. Macdonald, P. A. Cohen, F. Ö. Dudás, D. P. Schrag, Early neo-
709 proterozoic scale microfossils in the lower tindir group of alaska and the
710 yukon territory, *Geology* 38 (2010) 143–146.
- 711 [56] G. P. Halverson, F. A. Macdonald, J. V. Strauss, E. F. Smith, G. M.
712 Cox, L. Hubert-Théou, Updated definition and correlation of the lower
713 fifteenmile group in the central and eastern ogilvie mountains, Yukon
714 Exploration and Geology (2011) 75–90.
- 715 [57] F. A. Macdonald, P. A. Cohen, The tatonduk inlier, alaska–yukon bor-
716 der, *Geological Society, London, Memoirs* 36 (2011) 389–396.
- 717 [58] J. P. Pu, S. A. Bowring, J. Ramezani, P. Myrow, T. D. Raub, E. Land-
718 ing, A. Mills, E. Hodgins, F. A. Macdonald, Dodging snowballs:
719 Geochronology of the gaskiers glaciation and the first appearance of
720 the ediacaran biota, *Geology* 44 (2016) 955–958.
- 721 [59] D. Chew, C. Kirkland, The Chiquero Formation, southern Peru, 2011.

- 722 [60] F. A. Macdonald, D. S. Jones, Chapter 30 the khubsugul group, northern
723 mongolia 36 (2011) 339–345.
- 724 [61] F. A. Macdonald, D. S. Jones, D. P. Schrag, Stratigraphic and tectonic
725 implications of a newly discovered glacial diamictite–cap carbonate cou-
726 plet in southwestern mongolia, *Geology* 37 (2009) 123–126.
- 727 [62] R. P. Anderson, S. McMahon, U. Bold, F. A. Macdonald, D. E. Briggs,
728 Palaeobiology of the early ediacaran shuurgat formation, zavkhan ter-
729 rane, south-western mongolia, *Journal of Systematic Palaeontology* 15
730 (2017) 947–968.
- 731 [63] U. Bold, E. F. Smith, A. D. Rooney, S. A. Bowring, R. Buchwaldt, F. Ó.
732 Dudás, J. Ramezani, J. L. Crowley, D. P. Schrag, F. A. Macdonald,
733 Neoproterozoic stratigraphy of the zavkhan terrane of mongolia: The
734 backbone for cryogenian and early ediacaran chemostratigraphic records,
735 *American Journal of Science* 316 (2016) 1–63.
- 736 [64] S. B. Pruss, T. Bosak, F. A. Macdonald, M. McLane, P. F. Hoffman,
737 Microbial facies in a sturtian cap carbonate, the rasthof formation, otavi
738 group, northern namibia, *Precambrian Research* 181 (2010) 187–198.
- 739 [65] E. F. Smith, F. A. MacDonald, J. L. Crowley, E. B. Hodgkin, D. P.
740 Schrag, Tectonostratigraphic evolution of the c. 780–730 ma beck spring
741 dolomite: Basin formation in the core of rodinia, *Geological Society,*
742 London, Special Publications 424 (2016) 213–239.

- 743 [66] J. V. Strauss, A. D. Rooney, F. A. Macdonald, A. D. Brandon, A. H.
744 Knoll, 740 ma vase-shaped microfossils from yukon, canada: Implica-
745 tions for neoproterozoic chronology and biostratigraphy, *Geology* 42
746 (2014) 659–662.
- 747 [67] P. K. Strother, A. H. Knoll, E. S. Barghoorn, Micro-organisms from the
748 late precambrian narssâ rssuk formation, north-western greenland,
749 *Palaeontology* 26 (1983) 1–32.
- 750 [68] V. Sergeev, A. Knoll, P. Y. Petrov, Paleobiology of the mesoproterozoic-
751 neoproterozoic transition: the sukhaya tunguska formation, turukhansk
752 uplift, siberia, *Precambrian Research* 85 (1997) 201–239.
- 753 [69] V. N. Sergeev, A. H. Knoll, J. P. Grotzinger, Paleobiology of the meso-
754 proterozoic billyakh group, anabar uplift, northern siberia, *Journal of*
755 *paleontology* 69 (1995) 1–37.
- 756 [70] P. K. Pufahl, P. W. Fralick, Depositional controls on palaeoproterozoic
757 iron formation accumulation, gogebic range, lake superior region, usa,
758 *Sedimentology* 51 (2004) 791–808.
- 759 [71] A. H. Knoll, B. Simonson, Early proterozoic microfossils and penecon-
760 temporaneous quartz cementation in the sokoman iron formation,
761 canada, *Science* 211 (1981) 478–480.
- 762 [72] E. Perry, F. Tan, G. Morey, *Geology and stable isotope geochemistry of*

- 763 the biwabik iron formation, northern minnesota, *Economic Geology* 68
764 (1973) 1110–1125.
- 765 [73] J. P. Wilson, W. W. Fischer, D. T. Johnston, A. H. Knoll, J. P.
766 Grotzinger, M. R. Walter, N. J. McNaughton, M. Simon, J. Abelson,
767 D. P. Schrag, et al., Geobiology of the late paleoproterozoic duck creek
768 formation, western australia, *Precambrian Research* 179 (2010) 135–149.
- 769 [74] A. J. Bumby, P. G. Eriksson, O. Catuneanu, D. R. Nelson, M. J. Rigby,
770 Meso-archaeon and palaeo-proterozoic sedimentary sequence stratigra-
771 phy of the kaapvaal craton, *Marine and Petroleum Geology* 33 (2012)
772 92–116.
- 773 [75] A. Hofmann, R. Bolhar, B. Orberger, F. Foucher, Cherts of the bar-
774 berton greenstone belt, south africa: Petrology and trace-element geo-
775 chemistry of 3.5 to 3.3 ga old silicified volcanoclastic sediments, *South*
776 *African Journal of Geology* 116 (2013) 297–322.
- 777 [76] S. Kiyokawa, T. Ito, M. Ikehara, F. Kitajima, Middle archean volcano-
778 hydrothermal sequence: bacterial microfossil-bearing 3.2 ga dixon is-
779 land formation, coastal pilbara terrane, australia, *Geological Society of*
780 *America Bulletin* 118 (2006) 3–22.
- 781 [77] K. Sugitani, Strelley pool formation, *Encyclopedia of Astrobiology*
782 (2014) 1–7.

- 783 [78] B. M. Simonson, K. A. Schubel, S. W. Hassler, Carbonate sedimen-
784 tology of the early precambrian hamersley group of western australia,
785 Precambrian Research 60 (1993) 287–335.
- 786 [79] M. J. Van Kranendonk, Volcanic degassing, hydrothermal circulation
787 and the flourishing of early life on earth: A review of the evidence from
788 c. 3490-3240 ma rocks of the pilbara supergroup, pilbara craton, western
789 australia, Earth-Science Reviews 74 (2006) 197–240.

790 6. Supplementary Information

791 6.1. *geological descriptions*

792 1. The chert-rich, lime-mudstone and grey shale of the **Fifteenmile For-**
793 **mation**, exposed at Mt. Slipper in west-central Yukon, Canada is our
794 most heavily sampled unit [39]. This section is 810.7 ± 5.8 Ma according
795 Re-Os geochronology data on the organic rich shale horizon 4.15 meters
796 below the base of our section. Additionally, we report data from 7 sam-
797 ples from a parallel Fifteenmile section one kilometer along strike. This
798 section represents a mixed redox, semi-restricted basinal environment.
799 Samples were deposited below storm wave base in a distal slope setting.
800 Chert is present among all lithologies in the section, allochthonous and
801 autochthonous, but is variable in abundance, distribution, and form.
802 Four samples are specifically from the Hard Luck Creek outcrop and
803 are sourced from a yellow weathering dolomite with common intraclast
804 breccias, black chert nodules, shale interbeds, and molar tooth struc-
805 tures [55]. Like most other Neoproterozoic cherts these were peritidal
806 early replacement nodules. This group was intruded by mafic dikes,
807 but the samples are not taken from directly adjacent. Additional sam-
808 ples are from the peritidal reefal assemblage, a mixed carbonate shale
809 unit slightly lower in the section [56]. Two samples are from Mt Slip-
810 per, which are laterally correlative with the Hard Luck Creek samples.
811 These 2 samples are at the top of a dark gray limestone rhythmite
812 unit and are interpreted as subtidal in a shallowing upwards sequence.

813 These Yukon samples experienced Anchizone grade metamorphism cor-
814 responding to temperatures of 200-300 degrees as part of the orogeny
815 that formed the mountain range [57].

816 2. Data is provided from the **Rocky Harbour Formation** in Newfound-
817 land. These are chert clasts from a pistachio colored siliceous siltstone
818 located immediately above 579 Ma age Gaskiers glaciation diamictite
819 [58]. The siltstone contains wavy laminations and dewatering struc-
820 tures on a storm wave ripple surface indicating a deep water deposi-
821 tional environment.

822 3. Data is provided from the Neoproterozoic **San Juan Formation** in
823 southern Peru. The section has undergone greenschist facies metamor-
824 phism during an Early Paleozoic orogenesis [59]. Stratigraphically, the
825 measured sample (n=1) is immediately above the inferred Gaskiers cap
826 carbonate and represents the base of the Shuram anomaly. Litholog-
827 ically, the sample is from a limestone unit above a black shale. Due
828 to a lack of higher energy sedimentary structures this sample is most
829 likely deep marine, but bedding was subsequently disturbed indicating
830 possible alteration (Hodgin personal communication).

831 4. Data is presented from the **Khesen Formation** in Khubsugul, Mon-
832 golia. These units are peritidal, early replacement chert nodules that
833 precipitated in a dark grey limestone rhythmite. Stratigraphically this
834 unit sits above a glacial diamictite with its associated cap carbonate
835 and disconformably below a phosphorite deposit [60].

- 836 5. Data is presented from the **Zuune Arts Formation** in central Mongo-
837 lia. Samples were taken from a 100 meter thick unit of blue limestone
838 rhythmite and ribbonite. The same unit that includes the black chert
839 nodules also includes meandering ichnogenera. The oldest chert sample
840 from this unit (≈ 550 Ma) is a massive deepwater strataform, suggest-
841 ing the possible contribution of hydrothermal silica, while the younger
842 two samples (≈ 544 -545 Ma) are peritidal early replacement nodules
843 [61].
- 844 6. Data are presented from the **Shuurgat Formation**, a carbonate dom-
845 inated sequence located between the Zuune Arts Formation above and
846 the post-glacial Ol formation below. Deposition of chert nodules oc-
847 curred at the maximum flooding surface of a carbonate ramp. Based
848 on the presence of graded beds of flat-laminated micritic limestone with
849 minor grain flows of redeposited ooids these samples formed in a subti-
850 dal environment below fair-weather wave-base [62]. The compaction of
851 laminae surrounding the chert nodules indicate that the nodules formed
852 during early diagenesis.
- 853 7. Data are presented from the **Ol Formation**, a carbonate dominated
854 unit deposited immediately after the Marinoan Khongor diamictite.
855 This unit was deposited as part of a transgressive systems tract on an
856 isolated carbonate platform, analogous to the modern Bahama bank
857 [63]. This chert nodule is also a peritidal early replacement nodule,
858 but considering the conditions after the Marinoan may have formed

859 under higher-temperatures and equilibrated with low $\delta^{18}O$ meltwater
860 (Liljestrand, in prep).

861 8. Data are presented from the Cryogenian **Taishir Formation**, a largely
862 carbonate unit deposited between the Sturtian and Marinoan glacia-
863 tions. One sample is from a slightly older outcrop (≈ 660 Ma) of lime-
864 stone calcisiltite and thin-bedded micrite. The sedimentary structures
865 suggest this sample is an early replacement nodule from a sublittoral mi-
866 crobialite, slightly deeper than the common peritidal samples [63]. The
867 2 younger samples (≈ 650 Ma) are deposited in a calcsiltite unit above
868 a flooding surface. These samples are peritidal early replacement nod-
869 ules and were formed in the midst of a negative $\delta^{13}C$ excursion. Note,
870 these samples as well as the Ol, and Shuurgat, are part of the same
871 Taagaan Olom Group. It and the Zuune Arts formation located un-
872 conformably above were weakly metamorphosed as part of the Central
873 Asian Orogenic Belt (CAOB) [63].

874 9. Data are presented from the **Rasthof Formation** in Namibia. The
875 Rasthof is a carbonate sequence that immediately postdates the Stur-
876 tian diamictite and includes the cap dolostone as well as 200-400 meters
877 of dark gray rhythmite and microbialite [64]. There is no evidence for
878 wave action, which indicates this sample precipitated in the sublittoral
879 zone below wave base. The sample itself was taken from a microbialite
880 so it may be influenced by the climate immediately after snowball and
881 more localized biological processes.

- 882 10. Data are presented from the **Beck Springs Formation** in Death Val-
883 ley CA. The Beck Springs is a dolomite unit forming in a broadly
884 transgressive system [65]. The chert samples themselves are peritidal
885 early replacement nodules. Stratigraphically the Beck Springs immedi-
886 ately predates the Kingston Peak formation which is a diamictite that
887 has been correlated with the Marinoan glaciation.
- 888 11. Data are presented from the **Callison Lake Formation**, a mixed silici-
889 clastic and carbonate deposit located in the Yukon territory of Canada
890 dated to about 745 Ma. The chert samples themselves are sourced from
891 a dolostone unit characterized by abundant microbial lamination, do-
892 mal stromatolitic bioherms, and cross-bedded oolitic grainstone, as well
893 as the early diagenetic chert [66]. Callison Lake strata were formed in a
894 peritidal to shallow subtidal depositional environment in a periodically
895 restricted marginal marine basin.
- 896 12. Data are presented from the **Akademikerbreen Group**, a ≈ 750 Ma
897 Neoproterozoic unit in Svalbard, Norway. The Akademikerbreen group
898 is a 2000 meter succession that hosts a variety of carbonate facies.
899 Petrographic and microfossil evidence suggests that the silica nodules
900 replaced carbonate early in diagenesis, probably on a timescale no more
901 than a few thousand years [53]. Like other early diagenetic chert, these
902 samples probably formed in isolated evaporative coastal environments.
- 903 13. Data are presented from the ≈ 1200 Ma Aorferneq member of the
904 **Narssarssuk Formation** in northwest Greenland. The chert from

905 this unit are early diagenetic in origin, replacing preexisting carbonate
906 microbial mats. These samples likely formed in a broad and geologi-
907 cally relatively stable tidal flat environment varying from subtidal to
908 supratidal [67].

909 14. Data are presented from the **Sukhaya Tunguska Formation** in north-
910 western Siberia. This represents a 1000-1100 year old mixed limestone
911 and dolostone with abundant nodular chert. Chert show evidence of
912 early cementation and environments are largely semi-restricted periti-
913 dal with some subtidal and lower intertidal zones. [68]

914 15. Data are presented from the **Billyakh Group** in northern Siberia,
915 which samples the Kotiukan and the overlying Yusmastakh formation.
916 The Kotiukan samples are from a chert-rich layer in a broader unit
917 characterized by stromatolitic peritidal dolostones. The Yusmastakh
918 Formation is laminated to medium bedded dolomicrite with abundant
919 though not fossil-rich chert. The Billyakh cherts were likely formed in
920 peritidal environments, possibly semi-restricted and evaporative [69].

921 16. Data are presented from the ≈ 1860 Ma **Ironwood Iron Formation** in
922 Michigan. The Ironwood Formation is a Superior type iron formation
923 deposited on a relatively stable cratonic margin. The specific samples
924 are jaspery chert in a granular iron formation, indicating a relatively
925 shallow depositional environment, likely influenced by some current or
926 wave motion [70].

927 17. Data are presented from the ≈ 1860 Ma **Sokoman Iron Formation**

928 in Labrador, Canada. The Sokoman is composed of a variety of tex-
 929 tures and sedimentary structures [71]. These were likely deposited in
 930 relatively shallow water in contact with the open ocean and have been
 931 only lightly metamorphosed. Sokoman cherts are granular and show
 932 evidence of early silicification, making them more likely to preserve pri-
 933 mary isotopic signals [38]. Data are also presented from the **Wishart**
 934 **Formation**, which underlies the Sokoman Formation. The mineralogy
 935 and petrography of the sample is similar.

936 18. Data are presented from the ≈ 1860 Ma **Biwabak Iron Formation**
 937 in Minnesota. The outcrop has a stromatolitic texture which places a
 938 limit on the possible depth of deposition, primary chert has possibly
 939 been subsequently remineralized [72].

940 19. Data are presented from the ≈ 1860 Ma **Gunflint Iron Formation**
 941 in Ontario, Canada. The Gunflint is typical of early Proterozoic iron
 942 formations, one sample is clearly stromatolitic indicating a low energy
 943 shallow depositional environment, the other is more granular indicating
 944 a higher energy. The Gunflint Formation has experienced a low degree
 945 of metamorphic alteration and has abundant microfossils preserved [38].

946 20. Data are presented from the 1865 Ma **Duck Creek Formation**. The
 947 Duck Creek is primarily dolomite with minor associated iron formation.
 948 The sample comes from chert pods that are themselves associated with
 949 the iron formation [73].

950 21. Data are presented from the 2060 Ma **Franceville Group** in Gabon.

- 951 Not primarily an iron formation, instead this sample comes from a
952 stromatolitic black chert.
- 953 22. Data are presented from the 2709 Ma **Rietgat Formation** in the Ven-
954 tersdorp Supergroup in South Africa. The Ventersdorp Supergroup is
955 primarily volcanic, the Rietgat is a silicified carbonate located strati-
956 graphically between two flood basalt units. The sample is stromatolitic
957 in origin and probably represents a peritidal environment [74].
- 958 23. Data are presented from the 3250 Ma **Fig Tree Group** in South Africa.
959 The Fig Tree Gp. is a mixed shallow water and volcanic sequence. The
960 samples are from relatively minor banded iron formations [75].
- 961 24. Data are presented from the 3000 Ma **Cleaverville Formation** from
962 the George Creek Group in Australia. This sample is from a massive
963 chert bed, possibly deposited in a relatively deep subtidal environment
964 and silicified quickly. The unit is bounded by volcanic rocks, but has
965 experienced only low grade metamorphism [76].
- 966 25. Data are presented from the 2684 Ma **Jeerinah Formation** from the
967 Fortescue Group in Australia. The sample is from a carbonate unit
968 in the Jeerinah that immediately overlies a sandstone bed and pre-
969 cedes a black shale. The black chert formed as a replacement of the
970 carbonate and the formation has experienced minor low temperature
971 metamorphism.
- 972 26. Data are presented from the 3390 Ma **Strelley Pool Formation** in
973 Australia. The Strelley Pool formation covers a range of shallow water

974 to terrestrial depositional environments and associated lithologies. This
975 chert probably formed as an early diagenetic carbonate replacement in
976 a shallow water evaporitic environment [77].

977 27. Data are presented from the 3462 Ma **Kromberg Formation** in the
978 Onverwacht Group South Africa. The Kromberg formation has both
979 bedded (sampled here) and vein associated chert[75].

980 28. Data are presented from the 2550 Ma **Wittenoom Formation** from
981 the Hamersley Supergroup in Australia. The specific sample measured
982 here is a chert nodule in basinal carbonates. The sample is relatively
983 well preserved for an Archean age unit [78].

984 29. Data are presented from the **Tower and Apex formations**, both of
985 which are in the 3000 Ma Warrawoona Supergroup. The apex chert is
986 a minor phase bedded in a larger basalt unit, the Tower Formation is
987 immediately below the Apex Formation stratigraphically [79].

988 6.2. XRD information

989 Samples were analyzed at the University of Oxford on a Panalytical
990 Empyrean Series 2 powder X-ray diffractometer using a Co Ka source at
991 40 kV and 40 mA. Samples were prepared as randomly oriented aggregates
992 by mixing with ethanol and spread on zero background silicon single crys-
993 tal substrates. Background subtraction, peak statistics, phase identification,
994 and quantification were performed using HighScore Plus software. Quantifi-
995 cation was performed with the reference intensity ratio method using scale

996 factors recently compiled in the International Center for Diffraction Data
 997 (ICDD) Powder Diffraction File 4+.

998 *6.3. supporting figures*

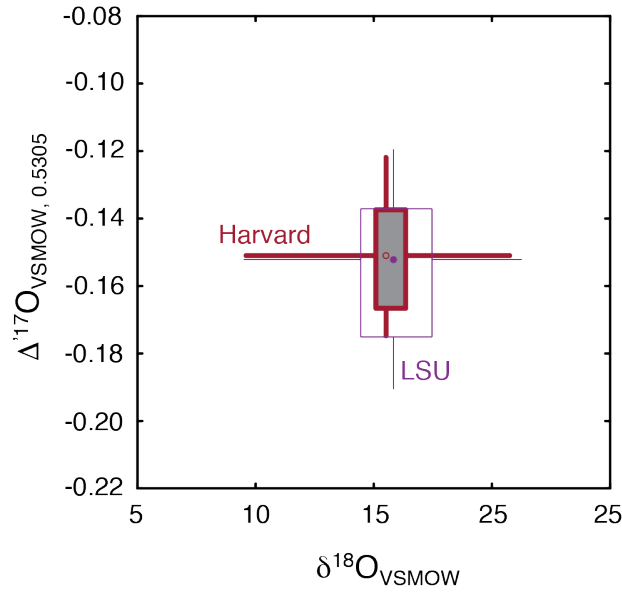


Figure S1: Comparison of $\delta^{18}\text{O}$ and $\Delta^{17}\text{O}$ for Archean chert samples that were measured at both LSU and Harvard. A) Shows the raw data with associated error bars of $\pm 0.019\text{‰}$ from Harvard and $\pm 0.023\text{‰}$. B) Shows the same data as a box and whisker plot to better compare the relative means. The points represent the means, the boxes represent 25-75 percentile, the whiskers represent the 5-95 percentile.

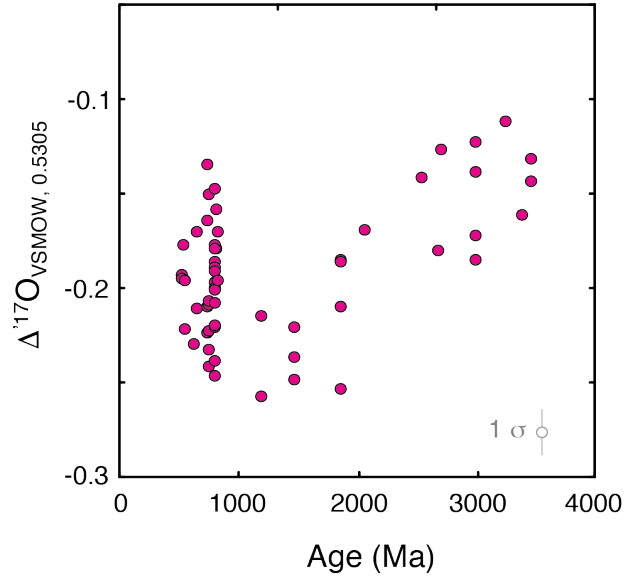


Figure S2: A plot of the mineralogically vetted $\Delta^{17}\text{O}$ compositions through time. Error is captured in the lower left of the frame.

| Sample ID | Age (Ma) | Origin | $\delta^{17}\text{O}$ | $\delta^{18}\text{O}$ | $\Delta^{17}\text{O}$ |
|---------------------------|----------|--------|-----------------------|-----------------------|-----------------------|
| See attached file. height | | | | | |

Table S1: Triple oxygen isotope data for Archean chert as measured at LSU and Harvard. All data is reported in ‰ units relative to VSMOW and $\Delta^{17}\text{O}$ values are normalized relative to $\lambda=0.5305$. Both datasets were normalized relative to the same literature values of San Carlos Olivine, NBS-28, and UWG-2. The mean difference between $\Delta^{17}\text{O}$ as measured at Harvard and LSU is 0.0012‰

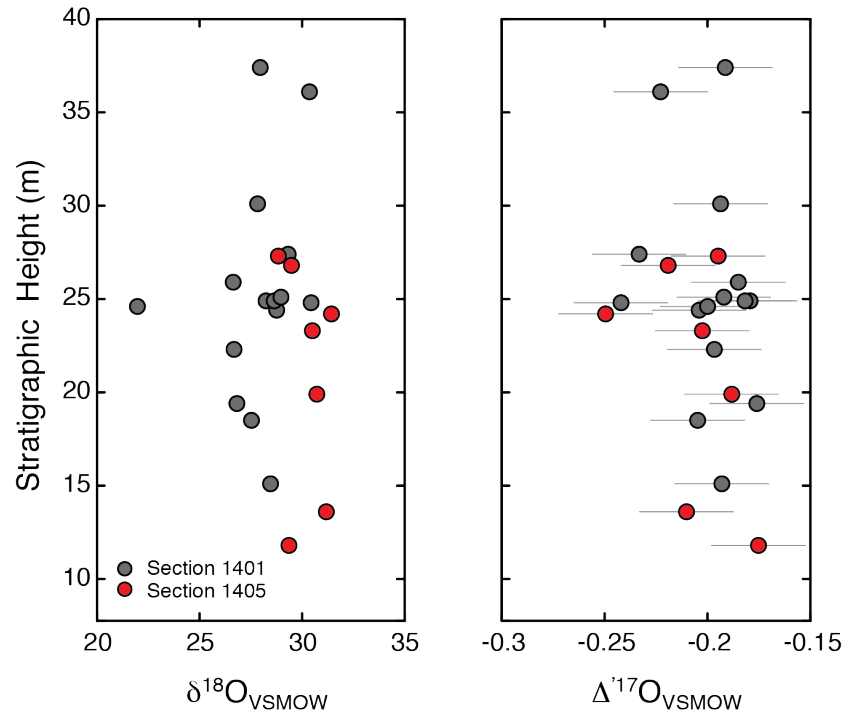


Figure S3: Oxygen isotope data of the stratigraphic test at the Fifteenmile formation. The red and gray data are from different parallel outcrops of the same formation. As can be seen, the oxygen isotope signal, especially in the minor isotope, is indistinguishable.

| | Raw mineralogy | | | | | | | After sample processing | | | | | | |
|---------------------------|----------------|-----------|-----------------|------------|--------|----------|--------------------|-------------------------|-----------|-----------------|------------|--------|----------|--------------------|
| | Quartz | Carbonate | Other Silicates | Phosphates | Oxides | Sulfates | Non Oxygen Bearing | Quartz | Carbonate | Other Silicates | Phosphates | Oxides | Sulfates | Non Oxygen Bearing |
| Sample ID | | | | | | | | | | | | | | |
| See attached file. height | | | | | | | | | | | | | | |

Table S2: Data from mineralogical analyses.

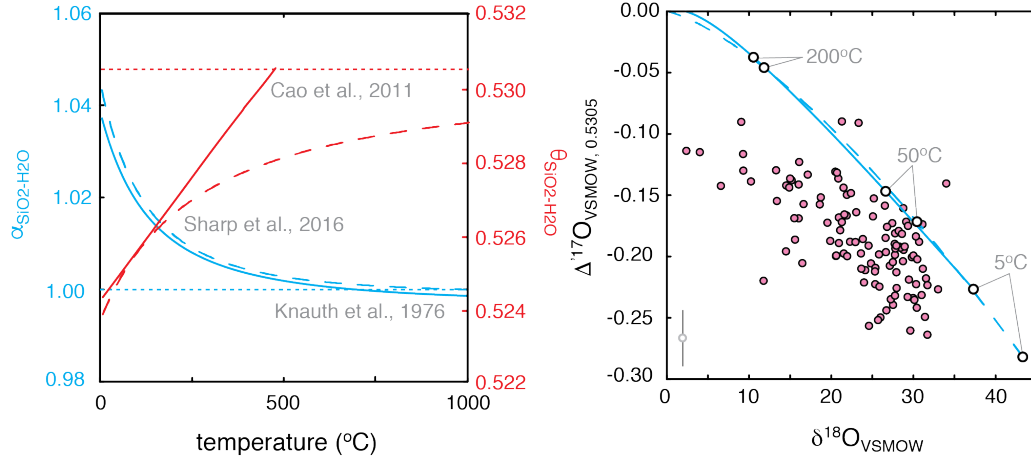


Figure S4: At left, we include the temperature dependent fractionation factors used in this analysis. At right, the model prediction with no diagenesis, no change in seawater chemistry, but changing surface temperatures (i.e. precipitation temperatures). Together these temperature predictions combine in $\Delta^{17}\text{O} - \delta^{18}\text{O}$ space to form concave down arrays that do not pass through the data. The different colored lines here represent the different temperature dependencies from the left frame.

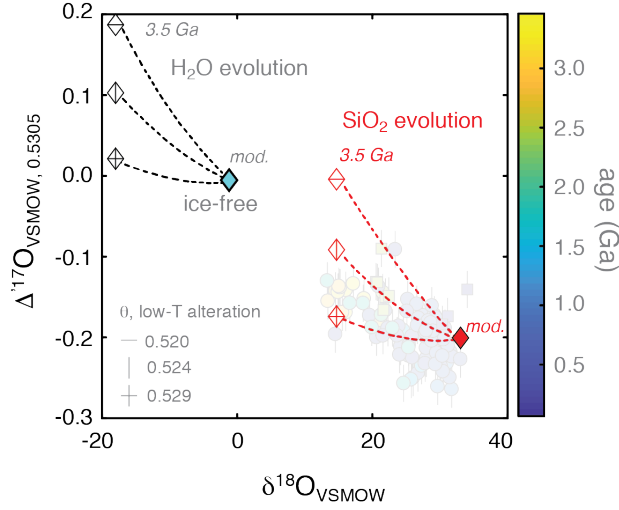


Figure S5: The triple isotope prediction associated with differential crustal interactions is sensitive to the choice of input fractionation factors. Here, we keep the 1.028 effect in $\delta^{18}\text{O}$, and explore the consequences for other values of θ . Note that 0.524 is the preferred values, based on measurements of oceanic crust [23]

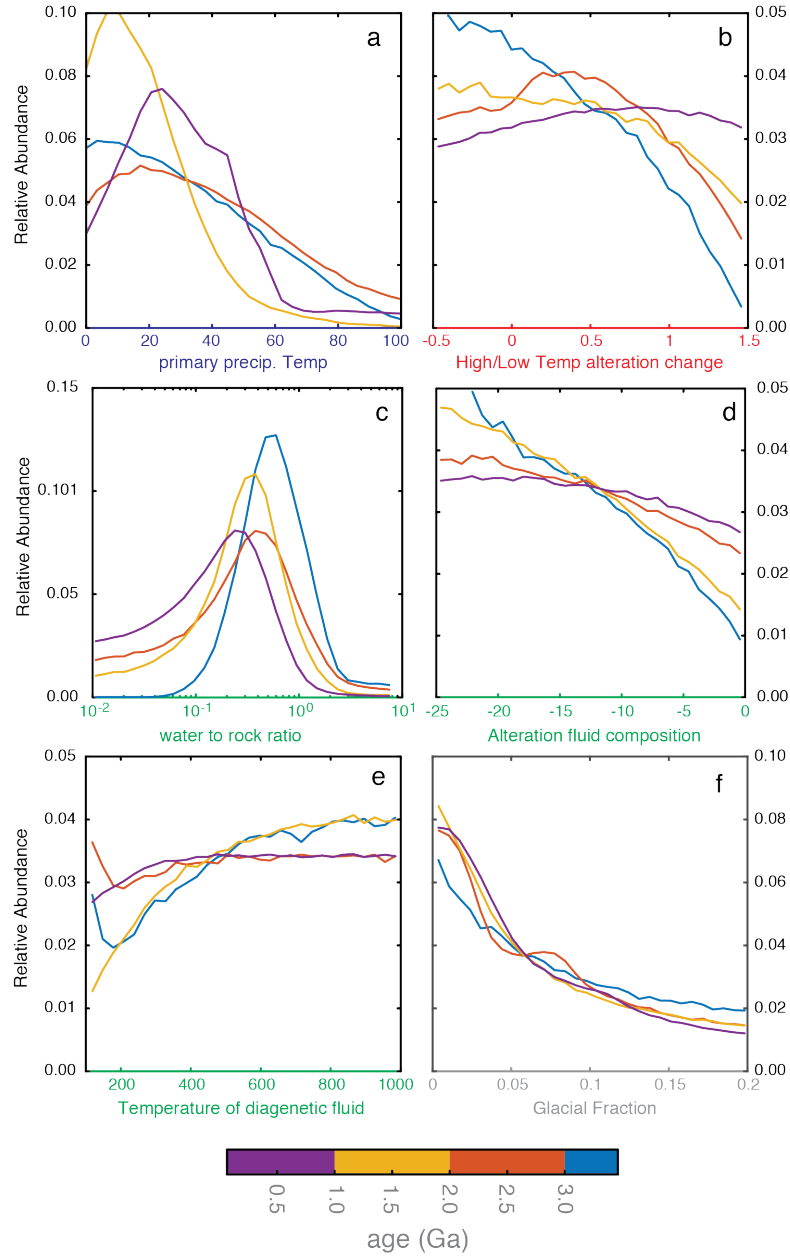


Figure S6: To evaluate whether building a bulk solution was losing information about temporal evolution, here we bin solutions by time, allowing for an additional layer of interpretation.

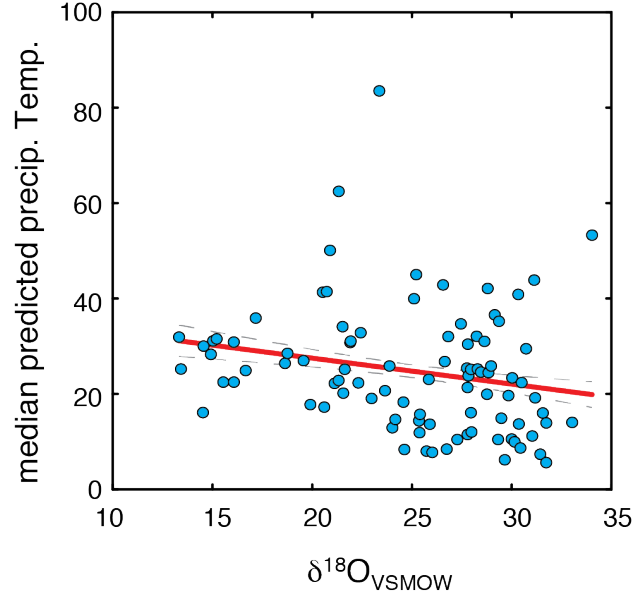


Figure S7: Measured $\delta^{18}\text{O}$ of the chert samples against the Monte Carlo predicted precipitation temperature. The statistics reflect the linear best fit for each dataset.

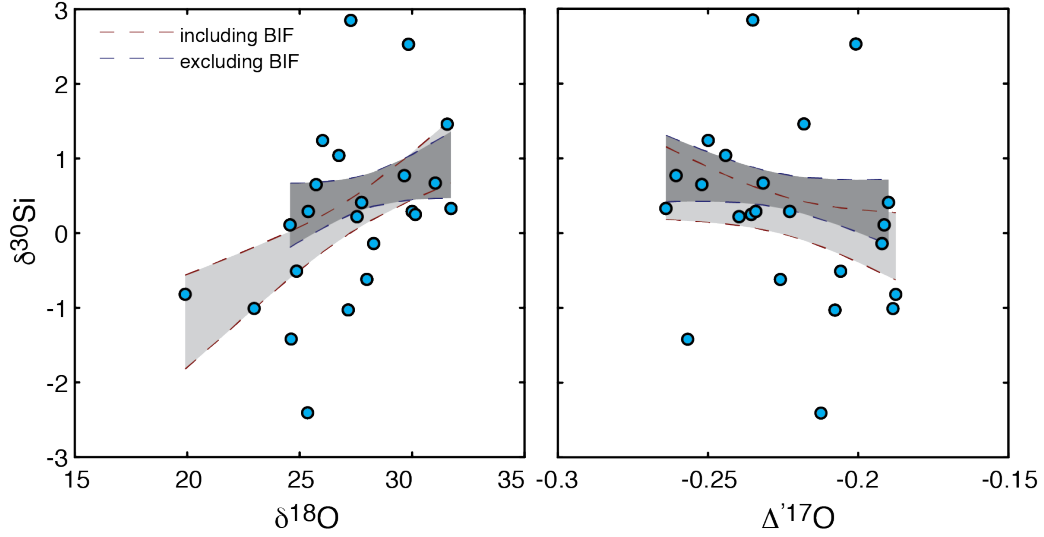


Figure S8: Comparison of the previously measured $\delta^{30}\text{Si}$ data with the new oxygen isotope compositions [53]. Red points are cherts associated with Paleoproterozoic BIF, Blue points are Proterozoic peritidal chert. The only statistically significant relationship ($P < 0.05$) exists between $\delta^{18}\text{O}$ and $\delta^{30}\text{Si}$ specifically when the BIF samples are included.

| Variable | Allowed Range | Description |
|-----------------------------------|---------------|---|
| ocean change fraction | -0.5 to 1.5 | The degree to which the ocean composition is allowed to evolve, held constant when at 0, follows described ocean change prediction when at 1, and scales proportionally for other values. |
| glacial fraction | 0 to 0.2 | Fraction of the ocean volume stored as ice, also approximates the degree of evaporation in an enclosed basin. |
| precipitation temperature | 0 to 100 | Equilibrium temperature at which the chert originally precipitates. Constrained to temperatures at which the ocean is liquid. |
| water to rock ratio | 0.01 to 10 | Defines the degree to which samples are altered, value can theoretically range from zero to infinity, but the three orders of magnitude here cover reasonable variability. |
| groundwater $\delta^{18}\text{O}$ | -25 to 0 | $\delta^{18}\text{O}$ Isotopic composition of groundwater with which alteration occurs. groundwater $\Delta^{17}\text{O}$ is constrained by this value according to the relationship described in Luz et al. 2010 [52]. |
| diagenesis temperature | 100 to 1000 | Equilibrium temperature at which the chert is diagenetically altered. Lower bound is set at 100 to ensure alteration always occurs at a temperature above original precipitation. |

Table S3: Variables included in the Monte Carlo model of chert formation

Table
Click here to download Table: Liljestrand_Data.xlsx

| ID | Age (Ma) | LSU Replicate 1 | | | | LSU Replica | |
|----------------|----------|-----------------------|-----------------------|---------------------------------|--------------------------------|-----------------------|-----------------------|
| | | $\delta^{18}\text{O}$ | $\delta^{17}\text{O}$ | $\Delta^{17}\text{O}_{-0.5305}$ | $\Delta^{17}\text{O}_{-0.528}$ | $\delta^{18}\text{O}$ | $\delta^{17}\text{O}$ |
| M602-607 a. | 525 | 14.52 | 7.48 | -0.196 | -0.160 | | |
| M602-607 b. | 525 | 21.56 | 11.18 | -0.198 | -0.144 | | |
| M620-1.1 a. | 540 | 16.52 | 8.52 | -0.206 | -0.165 | | |
| M620-1.1 b. | 540 | 15.63 | 8.07 | -0.186 | -0.148 | | |
| M622-169 | 544 | 23.39 | 12.16 | -0.179 | -0.121 | 26.82 | 13.98 |
| M622-146.5 | 545 | 20.10 | 10.57 | -0.047 | 0.003 | 26.63 | 13.90 |
| M622-85 a. | 550 | 25.84 | 13.43 | -0.198 | -0.135 | | |
| M622-85 b. | 550 | 25.90 | 13.43 | -0.225 | -0.161 | | |
| F726-165B a. | 600 | 23.75 | 12.32 | -0.208 | -0.150 | | |
| F726-165B b. | 600 | 23.65 | 12.28 | -0.198 | -0.139 | | |
| F723-58 a. | 632 | 16.13 | 8.40 | -0.123 | -0.083 | | |
| F723-58 b. | 632 | 27.79 | 14.41 | -0.232 | -0.164 | | |
| F704-330 a. | 650 | 19.56 | 10.16 | -0.173 | -0.124 | | |
| F704-330 b. | 650 | 20.37 | 10.54 | -0.214 | -0.163 | | |
| F704-331 a. | 650 | 22.32 | 11.59 | -0.188 | -0.133 | 20.84 | 10.82 |
| F704-331 b. | 650 | 20.97 | 10.88 | -0.189 | -0.137 | | |
| F702-100 | 660 | 24.02 | 12.45 | -0.221 | -0.162 | | |
| B1419-921.0 a. | 555 | 6.60 | 3.35 | -0.143 | -0.126 | | |
| B1419-921.0 b. | 555 | 11.73 | 5.98 | -0.227 | -0.198 | | |
| TP1 | 579 | 10.26 | 5.29 | -0.139 | -0.113 | | |
| TP2 | 579 | 9.05 | 4.70 | -0.089 | -0.067 | | |
| TP3 | 579 | 9.30 | 4.81 | -0.117 | -0.093 | | |
| F8013A a. | 660 | 23.07 | 12.01 | -0.164 | -0.107 | | |
| F8013A b. | 660 | 20.64 | 10.69 | -0.199 | -0.148 | | |
| F901-33.8 | 739 | 20.89 | 10.89 | -0.137 | -0.085 | | |
| F901-20 | 740 | 21.91 | 11.39 | -0.167 | -0.113 | | |
| F930_5.5 | 740 | 27.96 | 14.52 | -0.213 | -0.144 | | |
| F927-64.5 | 745 | 33.03 | 17.16 | -0.227 | -0.146 | | |
| F929_37.5 a. | 750 | 24.17 | 12.53 | -0.211 | -0.152 | | |
| F929_37.5 b. | 750 | 25.21 | 13.14 | -0.153 | -0.091 | | |
| 81B-550 | 750 | 28.12 | 14.61 | -0.209 | -0.140 | | |
| 86P-108-3 | 750 | 30.00 | 15.57 | -0.234 | -0.160 | 28.46 | 14.82 |
| 86P-96-2A | 750 | 30.14 | 15.64 | -0.236 | -0.161 | | |
| 81P-4705-2B | 750 | 26.74 | 13.85 | -0.244 | -0.178 | | |
| 81B-625-2A | 750 | 27.99 | 14.52 | -0.226 | -0.157 | | |
| T-714-1 | 770 | 27.16 | 14.11 | -0.208 | -0.141 | | |
| T-714-2 | 770 | 24.86 | 12.91 | -0.206 | -0.144 | | |
| T705-18 a. | 805 | 30.03 | 15.62 | -0.199 | -0.125 | | |
| T705-18 b. | 805 | 31.74 | 16.48 | -0.224 | -0.145 | | |
| T705-18 c | 820 | 29.15 | 15.19 | -0.172 | -0.100 | | |
| T705-154.2 | 812 | 27.80 | 14.47 | -0.181 | -0.113 | | |
| T705-123.6 | 815 | 28.80 | 15.01 | -0.161 | -0.090 | | |
| P1405-11.8 | 810.7 | 29.42 | 15.35 | -0.150 | -0.077 | | |
| P1405-13.6 | 810.7 | 31.18 | 16.21 | -0.210 | -0.133 | | |

LaTeX Source Files

[Click here to download LaTeX Source Files: The Geologic Record of \$\\$^{17}\$ \(1\).zip](#)

Author declaration

[Instructions: Please check all applicable boxes and provide additional information as requested.]

1. Conflict of Interest

Potential conflict of interest exists:

X ☐ No conflict of interest exists.

We wish to confirm that there are no known conflicts of interest associated with this publication and there has been no significant financial support for this work that could have influenced its outcome.

2. Funding

☐ Funding was received for this work.

All of the sources of funding for the work described in this publication are acknowledged below:

[List funding sources and their role in study design, data analysis, and result interpretation]

X No funding was received for this work.

3. Intellectual Property

X We confirm that we have given due consideration to the protection of intellectual property associated with this work and that there are no impediments to publication, including the timing of publication, with respect to intellectual property. In so doing we confirm that we have followed the regulations of our institutions concerning intellectual property.

4. Research Ethics

X We further confirm that any aspect of the work covered in this manuscript that has involved human patients has been conducted with the ethical approval of all relevant bodies and that such approvals are acknowledged within the manuscript.

☐ IRB approval was obtained (required for studies and series of 3 or more cases)

☐ Written consent to publish potentially identifying information, such as details or the case and photographs, was obtained from the patient(s) or their legal guardian(s).

5. Authorship

The International Committee of Medical Journal Editors (ICMJE) recommends that authorship be based on the following four criteria:

1. Substantial contributions to the conception or design of the work; or the acquisition, analysis, or interpretation of data for the work; AND
2. Drafting the work or revising it critically for important intellectual content; AND
3. Final approval of the version to be published; AND
4. Agreement to be accountable for all aspects of the work in ensuring that questions related to the accuracy or integrity of any part of the work are appropriately investigated and resolved.

All those designated as authors should meet all four criteria for authorship, and all who meet the four criteria should be identified as authors. For more information on authorship, please see <http://www.icmje.org/recommendations/browse/roles-and-responsibilities/defining-the-role-of-authors-and-contributors.html#two>.

☒ All listed authors meet the ICMJE criteria. We attest that all authors contributed significantly to the creation of this manuscript, each having fulfilled criteria as established by the ICMJE.

☐ One or more listed authors do(es) not meet the ICMJE criteria.

We believe these individuals should be listed as authors because:

☒ We confirm that the manuscript has been read and approved by all named authors.

☒ We confirm that the order of authors listed in the manuscript has been approved by all named authors.

6. Contact with the Editorial Office

The Corresponding Author declared on the title page of the manuscript is:

DAVID JOHNSTON

XThis author submitted this manuscript using his/her account in EVISE.

XWe understand that this Corresponding Author is the sole contact for the Editorial process (including EVISE and direct communications with the office). He/she is responsible for communicating with the other authors about progress, submissions of revisions and final approval of proofs.

XWe confirm that the email address shown below is accessible by the Corresponding Author, is the address to which Corresponding Author's EVISE account is linked, and has been configured to accept email from the editorial office of American Journal of Ophthalmology Case Reports:

johnston@eps.harvard.edu

☐ Someone other than the Corresponding Author declared above submitted this manuscript from his/her account in EVISE:

[Insert name below]

☐ We understand that this author is the sole contact for the Editorial process (including EVISE and direct communications with the office). He/she is responsible for communicating with the other authors, including the Corresponding Author, about progress, submissions of revisions and final approval of proofs.

We the undersigned agree with all of the above.

Author's name (First, Last)

Signature

Date



1. David Johnston

—

_____ 10/22/2019

Author contributions statement:

Frasier L. Liljestrand and David T. Johnston: conceptualization, modeling

Frasier L. Liljestrand, David Johnston, Yongbo Peng, Nick Tosca: data collections and analysis.

Phoebe A. Cohen, Francis A. Macdonald, Andrew H. Knoll: sample curation

All authors contributed to the writing of this manuscript.